The ESSENCE Supernova Survey: Survey Optimization, Observations, and Supernova Photometry

G. Miknaitis[1], G. Pignata[2], A. Rest[3], W. M. Wood-Vasey[4], S. Blondin[4], P. Challis[4],
R. C. Smith[3], C. W. Stubbs[4,5], N. B. Suntzeff[3,6], R. J. Foley[7], T. Matheson[8], J. L. Tonry[9],
C. Aguilera[3], J. W. Blackman[10], A. C. Becker[11], A. Clocchiatti[2], R. Covarrubias[11],
T. M. Davis[12], A. V. Filippenko[7], A. Garg[4,5], P. M. Garnavich[13], M. Hicken[4,5], S. Jha[7,13],
K. Krisciunas[13,6], R. P. Kirshner[4], B. Leibundgut[14], W. Li[7], A. Miceli[11], G. Narayan[4,5],
J. L. Prieto[15], A. G. Riess[16,17], M. E. Salvo[10], B. P. Schmidt[10], J. Sollerman[12,18],
J. Spyromilio[14], A. Zenteno[3]

gm@fnal.gov

ABSTRACT

We describe the implementation and optimization of the ESSENCE supernova survey, which we have undertaken to measure the equation of state parameter of the dark energy. We present a method for optimizing the survey exposure times and cadence to maximize our sensitivity to the dark energy equation of state parameter $w = P/\rho c^2$ for a given fixed amount of telescope time. For our survey on the CTIO 4m telescope, measuring the luminosity distances and redshifts for

[1]Fermi National Accelerator Laboratory, P.O. Box 500, Batavia, IL 60510-0500

[2]Pontificia Universidad Católica de Chile, Departamento de Astronomía y Astrofísica, Casilla 306, Santiago 22, Chile

[3]Cerro Tololo Inter-American Observatory, National Optical Astronomy Observatory, Casilla 603, La Serena, Chile

[4]Harvard-Smithsonian Center for Astrophysics, 60 Garden Street, Cambridge, MA 02138

[5]Department of Physics, Harvard University, 17 Oxford Street, Cambridge, MA 02138

[7]Department of Astronomy, 601 Campbell Hall, University of California, Berkeley, CA 94720-3411

[8]National Optical Astronomy Observatory, 950 North Cherry Avenue, Tucson, AZ 85719-4933

[9]Institute for Astronomy, University of Hawaii, 2680 Woodlawn Drive, Honolulu, HI 96822

[10]The Research School of Astronomy and Astrophysics, The Australian National University, Mount Stromlo and Siding Spring Observatories, via Cotter Road, Weston Creek, PO 2611, Australia

[11]Department of Astronomy, University of Washington, Box 351580, Seattle, WA 98195-1580

[12]Dark Cosmology Centre, Niels Bohr Institute, University of Copenhagen, Juliane Maries Vej 30, DK-2100 Copenhagen Ø, Denmark

[13]Department of Physics, University of Notre Dame, 225 Nieuwland Science Hall, Notre Dame, IN 46556-5670

[13]Kavli Institute for Particle Astrophysics and Cosmology, Stanford Linear Accelerator Center, 2575 Sand Hill Road, MS 29, Menlo Park, CA 94720

[6]Department of Physics, Texas A&M University, College Station, TX 77843-4242

[14]European Southern Observatory, Karl-Schwarzschild-Strasse 2, D-85748 Garching, Germany

[15]Department of Astronomy, Ohio State University, 4055 McPherson Laboratory, 140 West 18th Avenue, Columbus, OH 43210

[16]Space Telescope Science Institute, 3700 San Martin Drive, Baltimore, MD 21218

[17]Johns Hopkins University, 3400 North Charles Street, Baltimore, MD 21218

[18]Department of Astronomy, Stockholm University, AlbaNova, 10691 Stockholm, Sweden

supernovae at modest redshifts ($z \sim 0.5 \pm 0.2$) is optimal for determining w. We describe the data analysis pipeline based on using reliable and robust image subtraction to find supernovae automatically and in near real-time. Since making cosmological inferences with supernovae relies crucially on accurate measurement of their brightnesses, we describe our efforts to establish a thorough calibration of the CTIO 4m natural photometric system.

In its first four years, ESSENCE has discovered and spectroscopically confirmed 102 type Ia SNe, at redshifts from 0.10 to 0.78, identified through an impartial, effective methodology for spectroscopic classification and redshift determination. We present the resulting light curves for the all type Ia supernovae found by ESSENCE and used in our measurement of w, presented in Wood-Vasey et al. (2007).

Subject headings: cosmology: observations — supernovae — surveys — methods: data analysis

1. Introduction

This is a report on the first four years of the ESSENCE survey (Equation of State: SupErNovae trace Cosmic Expansion), a program to measure the cosmic equation of state parameter to a precision of 10% through the discovery and monitoring of high redshift supernovae. The motivations and goals of ESSENCE, as well as the methods and data are presented here. ESSENCE is part of the exploration of the new and surprising picture of an accelerating universe, which has become the prevailing cosmological paradigm. This paradigm is supported by essentially all current observations, including those based on supernova distances, the large scale clustering of matter, and fluctuations in the cosmic microwave background. The free parameters of this concordance model can consistently fit these diverse and increasingly precise measurements.

This paper describes the survey design and optimization, and the acquisition and photometric analysis of our data through to the generation of photometrically calibrated SN light curves. The companion paper by Wood-Vasey et al. (2007) describes how luminosity distances are measured from the SN light curves and derives constraints on w from the ESSENCE observations.

1.1. Cosmology and Dark Energy

While the current observational agreement on a concordance model is surprisingly good (Tegmark et al. 2004; Eisenstein et al. 2005; Spergel et al. 2006), it comes at the high cost of introducing two unknown forms of mass-energy: non-baryonic dark matter and dark energy that exerts negative pressure. Each is a radical idea, and it is only because multiple independent observations require their existence that we have come to seriously consider new physics to account for these astronomical phenomena.

The dark energy problem is currently one of the most challenging issues in the physical sciences. The stark difference between the staggeringly *large* value for the vacuum energy predicted by quantum field theory and the cosmic vacuum energy density inferred from observations leads us to wonder how this vacuum energy of the Universe could be so *small* (Weinberg 1989; Carroll et al. 1992; Padmanabhan 2003; Peebles & Ratra 2003). On the other hand the convergence of observations that give rise to the ΛCDM concordance cosmology, with $\Omega_\Lambda \sim 0.7$ rather than identically zero, forces us to ask why the vacuum energy is so large.

More broadly, these cosmological observations can be interpreted as evidence for physics beyond our standard models of gravitation and quantum field theory. It is perhaps no coincidence that this occurs at the friction point between these two independently successful, but as yet unmerged paradigms. Our understanding of the gravitational implications of quantum processes appears to be incomplete at some level.

The dark energy problem challenges us on many fronts: theoretical, observational and experimental. Observational cosmology has an important role to play, and the current challenge is to undertake measurements that will lead to a better understanding of the nature of the dark energy (Albrecht et al. 2006). In particular we seek to measure the equation of state parameter $w = P/\rho c^2$ of the dark energy, as this can help us test theoretical models. One specific goal is to establish whether the observed accelerating expansion of the Universe is due to a classical cosmological constant or some other new physical process.

Within the framework of Friedmann-Robertson-Walker cosmology, the only way to reconcile the observed geometric flatness and the observed matter density is through another component of mass-energy that does not clump with matter. The observation of acceleration from supernovae is the unique clue that indicates this component must have negative pressure (Riess et al. 1998; Perlmutter et al. 1999; Riess et al. 2001; Tonry et al. 2003; Knop et al. 2003; Barris et al. 2004; Riess et al. 2004; Clocchiatti et al. 2006; Astier et al. 2006; Riess et al. 2006). As the evidence from supernovae has grown more conclusive, the intellectual focus has shifted from verifying the existence of dark energy to constraining its

properties (Freedman & Turner 2003). Accordingly, several large-scale, multi-year super-nova surveys have embarked on studying dark energy by collecting large, homogenous data sets. The Supernova Legacy Survey has published cosmological constraints using 73 SNe from its first year sample (Astier et al. 2006) between redshifts 0.2 and 1.0, and it continues to accumulate data. More recently, SDSS-II Supernova Survey (Frieman et al. 2004) has observed ~ 200 supernovae at redshifts out to 0.4. The final supernova samples from each of these programs and ESSENCE will each number in the hundreds.

Of the various models for dark energy currently being discussed in the literature, the cosmological constant (i.e. some uniform vacuum energy density) holds a special place, as both the oldest, originating with Einstein, and, in many ways, the simplest (Carroll et al. 1992). Quantum field theory suggests how to calculate the energy of the vacuum, but there is no plausible theoretical argument that accounts for the small, but non-zero, value required by observations. A host of other alternatives has been proposed, many of which appeal to slowly rolling scalar fields, similar to those used to describe inflation. Such models readily produce predictions that agree with the current observational results, but suffer from a lack of clear physical motivation, being concocted after the fact to solve a particular problem. Another class of ideas appeals to higher dimensional "brane world" physics inspired by string theory; for example, the cyclic universe (Steinhardt & Turok 2002, 2005) or modifications to gravity due to the existence of extra dimensions (Dvali et al. 2003).

One straightforward way to parameterize the dark energy is by assuming its equation of state takes the form $P = w\rho c^2$, where P and ρ are pressure and density respectively, related by an "equation-of-state" parameter w. Non-relativistic matter has $w = 0$, while radiation has $w = +1/3$, and different proposed explanations for the dark energy have a variety of values of w. In general, to produce an accelerated expansion, a candidate dark energy model must have $w < -1/2$ for a current matter density of $\Omega_M \sim 1/3$. The classical cosmological constant, Λ, of General Relativity has an equation-of-state parameter $w = -1$ exactly, at all times. Other models can take on a variety of effective w values that may vary with time. For example, quintessence (Steinhardt 2003) posits a minimally coupled rolling scalar field, with an equation of state,

$$w \sim \frac{P}{\rho} = \frac{\frac{1}{2}\dot{\phi}^2 - V(\phi)}{\frac{1}{2}\dot{\phi}^2 + V(\phi)}. \tag{1}$$

In this case, the effective value of w depends on the form of the potential chosen and can evolve over time. In general the parameterization of dark energy in terms of w is a convenient and useful tool to compare a variety of models (Weller & Albrecht 2002).

As a first step towards determining the nature of dark energy, the obvious place to start is to test whether the observed w is consistent with -1 (Garnavich et al. 1998). If not, then

a cosmological constant is ruled out as the explanation for dark energy.

If w is measured to be consistent with -1, then while models that exhibit an effective $w \sim -1$ are still allowed, the range in parameter space in which they can exist will be significantly restricted. Breaking the degeneracy between Λ and such "impostors" would then require measurements of the additional parameters that describe their time dependence. However, the form of such a parameterization is at present largely unrestricted and the choice of arbitrary parameterizations influences the conclusions derived from the analysis of the data (Upadhye et al. 2005). In the future, measurements of growth of structure, such as through weak lensing surveys, will provide a powerful complement to supernova measurements in constraining the properties of dark energy, as well as checking for possible modifications to General Relativity (Albrecht et al. 2006). In the near term, constraining w under the assumption that it is constant allows us to test a well-posed hypothesis that can be addressed with existing facilities and methods. While under standard General Relativity, w is bounded by the null dominant energy condition to be greater than or equal to -1, we should keep an open mind as to whether the data allow $w < -1$, since dark energy may well arise from physics beyond today's standard theories.

Motivated by these considerations, we have undertaken a project to use type Ia supernovae to measure w with a target fractional uncertainty of 10%. Observations of type Ia supernovae provided the first direct evidence for accelerating cosmic expansion, and they remain an incisive tool for studying the properties of the dark energy.

1.2. Measuring the physics of dark energy with supernovae

Type Ia supernovae (SNe Ia) are among the most energetic stellar explosions in the universe. Their high peak luminosities $(4-5\times10^9 L_\odot)$ make SNe Ia visible across a large fraction of the observable universe. The peak luminosity can be calibrated to $\sim 15\%$ precision in flux (Phillips 1993; Hamuy et al. 1996; Riess et al. 1996; Goldhaber et al. 2001; Guy et al. 2005; Jha et al. 2007). They are thus well suited to probing the expansion history during the epoch in which the Universe has apparently undergone a transition from deceleration to acceleration $(0 < z < 1)$. The utility of SNe Ia as "standardizable" candles was established observationally by Phillips (1993), with the identification of a correlation between peak luminosity and width of the light curves. The "type Ia" designation is an observational distinction, denoting objects whose spectra lack hydrogen or helium features, but exhibit a characteristic absorption feature observed at $\lambda6150$, but attributed to Si II $\lambda6355$. These objects are now thought to be the thermonuclear disruption of a carbon-oxygen white dwarf at or near the Chandrasekhar mass (Hoyle & Fowler 1960), with accretion from a companion star. Material gained through accretion pushes the total mass of the C-O WD above what can be supported by degeneracy pressure and results in nuclear burning, which eventually results in a powerful burning wave that completely destroys the star. A large fraction of the progenitor burns rapidly to produce ^{56}Ni, whose radioactive decay then powers the observed light curve (Colgate & McKee 1969). Bolometric light curves suggest that $\sim 0.7 M_\odot$ of ^{56}Ni is produced, which suggests that the burning is incomplete (Contardo et al. 2000; Stritzinger et al. 2006). There is disagreement on important details of whether the burning wave is supersonic (a detonation) or purely subsonic (a deflagration) (Hillebrandt & Niemeyer 2000). Nevertheless, models for the explosion give broad agreement with the observed light curves and spectra, though the specifics of progenitors and explosion physics remain unresolved (Branch et al. 1995; Renzini 1996; Nomoto et al. 2000; Livio 2000).

Fortunately, so far the lack of a detailed understanding of supernova physics has not prohibited the use of these objects as probes of cosmology, as the empirical correlations of light curve shape and color with luminosity appear to largely "standardize" supernovae. Subtle effects such as how supernovae are connected to stellar populations and how those populations may change with time and chemical composition will certainly become important in the future as we attempt to place ever tighter constraints on dark energy (Hamuy et al. 2000; Jha 2002; Gallagher et al. 2005; Sullivan et al. 2006). For example, observations suggest that the brightest SNe Ia are found only in galaxies with current star formation.

As in classical physics, the flux density from a cosmological source falls off as the inverse

square of distance,

$$\mathcal{F} = \frac{L}{4\pi D_l^2}.$$ (2)

However, this luminosity distance, D_l, depends upon how the universe expands as a photon travels from emitter to receiver, which in turn depends sensitively on the composition and properties of the constituents of the cosmic mass-energy density. Specifically, for a flat universe the luminosity distance, $D_l(z)$, is given by

$$D_l = \frac{c(1+z)}{H_0} \int_0^z \frac{1}{\sqrt{(1-\Omega_M)(1+z')^{3(1+w)} + \Omega_M(1+z')^3}} dz',$$ (3)

where w is taken here to be constant. In cosmological analyses, the combination of the Hubble constant and the intrinsic luminosity of SNe Ia is a multiplicative nuisance parameter which scales distance measurements at all redshifts by the same amount. Thus, under the assumption of flatness, $\Omega_M + \Omega_X = 1$, when measuring w, the only other free cosmological parameter is the matter density, Ω_M.

If we seek to constrain w using the luminosity distance-redshift test, it is worth considering which redshifts are most incisive. The relative differences in distance modulus as a function of redshift, for different values of w, are shown in Figure 1, where Ω_M and Ω_Λ have been fixed at 0.3 and 0.7 respectively.

There is a significant w-dependent signal even at intermediate redshifts ($z \sim 0.4$), at which observations with a 4-meter class telescope can readily yield many supernovae each month. Of course, observations such as the ESSENCE survey actually produce a complex set of constraints in cosmological parameter space, but much of the signal of interest is readily accessible at intermediate redshifts, between 0.3 and 0.8.

1.3. Considerations for optimally constraining w with SNe Ia observations

We wish to determine the optimal use of the time allocated for the ESSENCE survey on the Blanco 4m for constraining w. For a ground-based survey, a variety of factors determine the number of useful supernovae monitored, and the uncertainties associated with each data point on the light curve. The overall quality of each supernova light curve, in turn, determines the precision of its luminosity distance. Some of factors which impact the ability of a particular survey strategy to constrain cosmological parameters include:

- *Typical site conditions:* Seeing, weather, sky background, atmospheric transmission.
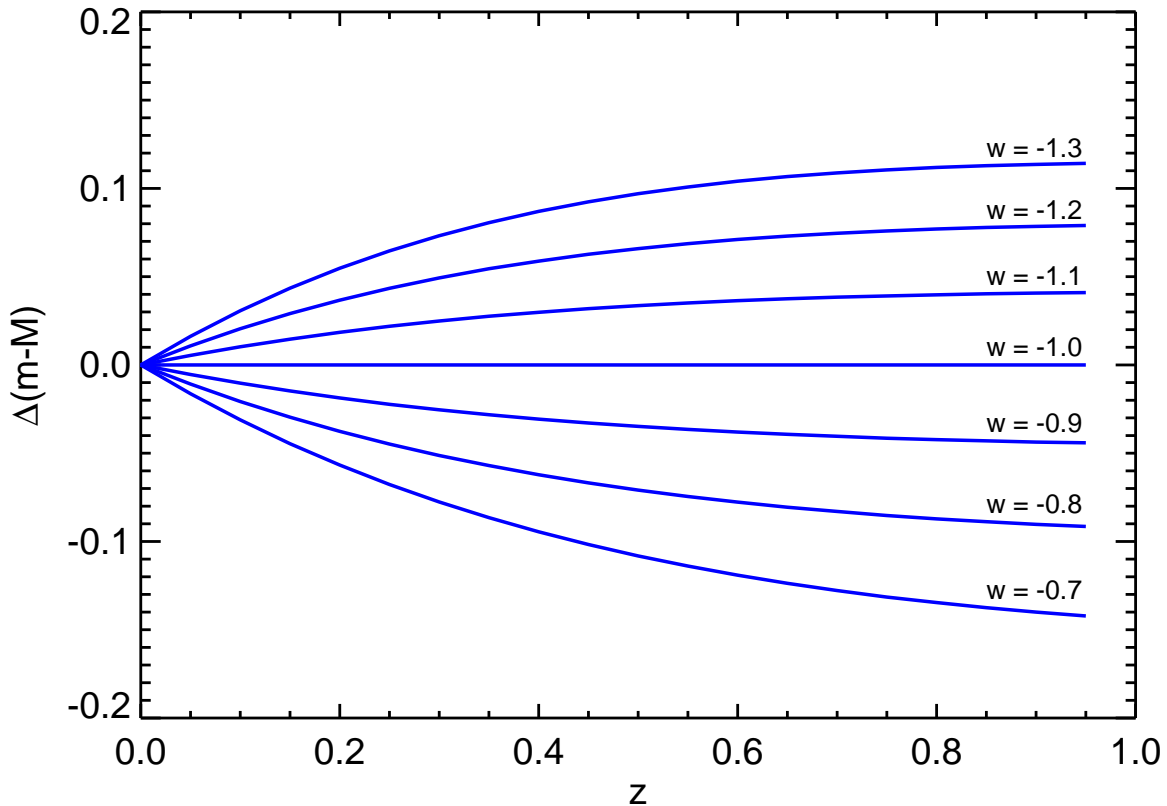
Fig. 1.— Differences in distance modulus for different values of w as a function of redshift, relative to $w = -1$, for $\Omega_m = 0.3, \Omega_\Lambda = 0.7$. Note that even at modest redshifts there is a significant fraction of the total asymptotic signal available.

- *System throughput vs. wavelength:* Aperture, optics, field of view, detector quantum efficiency.

- *Temporal constraints*: Telescope scheduling constraints, camera readout time.

- *SNR considerations*: Requisite S/N ratio and cadence required for distance determination.

- *Passband considerations*: Number of bands needed for extinction and SN color discrimination.

- *Spectroscopic considerations:* Location, availability and scheduling of followup spectroscopic resources

In order to optimize the observational survey strategy for ESSENCE, we tried to parameterize several of the factors above and balance them to obtain the strongest constraints on w. With the strong cosmological signal available in the redshift range from 0.3 to 0.8, it is clear that a wide-field camera on a 4m-class telescope can provide the needed balance of photometric depth (SNe Ia have m∼22 at peak at z=0.5) and sky coverage. Smaller fields of view on larger telescopes are better suited to going to higher redshifts, while wider fields on smaller telescopes are only able to reach redshifts where the cosmological signal is small. Combining these criteria with the range of spectroscopic followup facilities available to our collaboration, we quickly focused our analyses on the Blanco 4m telescope at CTIO together with the MOSAIC camera as providing an optimal combination of site (seeing plus weather), aperture, field of view, and telescope scheduling.

Beyond the selection of appropriate telescopes and instrumentation, there are relatively few "free parameters" controllable by the observers. These include the optical passbands used, the exposure time in each passband for each field, the total number of fields monitored, the cadence of the repeated observations, and ability to obtain spectra for each supernova candidate.

Using existing knowledge of the distribution of supernova magnitudes and colors as a function of redshift and time after explosion, we can relate the exposure times in different passbands, for a given desired signal-to-noise ratio (SNR). The calibration of luminosity from light curve shape is currently best understood in rest-frame B and V passbands. These passbands map to observer-frame R and I for supernovae at $z \sim 0.4$ (i.e. the uncertainties in k-corrections (Nugent et al. 2002) are small). For supernovae at these redshifts, observations taken in R and I, with the I band exposure time equal to twice that in R, are sufficient to match the SNR in both bands and measure distances to the SNe Ia.

While observations in a third bandpass would aid in determination of color, and thus, the estimates of extinction in the host galaxies, such observations would require significant additional observing time and are not easily accommodated within our optimization of limited observing time, photometric depth, sky coverage, and number of resulting SNe. Acquiring V band observations would provide a better match to rest-frame B for low redshift supernovae, but supernovae in our sample will be bright and have well-measured colors at these redshifts. Observations in the z-band would aid the color determination at higher redshifts, but the low quantum efficiency of of the MOSAIC CCD detectors, as well as the brightness of the night sky in this band and the heavy fringing due to night-sky emission lines make obtaining useful data in this band impractical.

Therefore, by limiting our strategy to R and I and demanding that I band exposure times scale with R band exposure time, the survey optimization problem then is reduced to

considering a single free parameter: the distribution of R band integration times across the survey fields for a given fixed amount of telescope time. What is the balance between survey depth (which extends the redshifts probed) and area (which increases the area covered each redshift slice)?

Consider the cosmological information contained in a single, perfect measurement of distance and redshift. Under the assumption of flat geometry (and with perfect knowledge of H_0 and the intrinsic luminosity of SNe Ia), each such measurement traces out a curve of allowable values of Ω_{M} and w , as shown in Figure 2. It is clear that if the goal is to measure w from SNe Ia alone, a large span in redshift is desirable in order to maximize the orthogonality of the curves and break the degeneracy between matter density and the equation-of-state parameter.

However, because the difference between these curves is small even over a large span in redshift, such a measurement would require massive numbers of SNe Ia achievable only by next generation experiments, such as the DES, PanSTARRS, LSST or JDEM. In the near term, we may appeal to other cosmological measurements to provide a constraint on Ω_m, such as from large scale structure measurements. This affords us some freedom in the redshifts at which we make our measurements, since the constraints from distance measurements are nearly orthogonal to an Ω_m prior of ~ 0.3 at all redshifts. [1] Though the sensitivity to differences in cosmological models is weaker at lower redshifts, there is a powerful observational advantage to working there, because obtaining good photometric and spectroscopic measurements is far cheaper in units of telescope time.

To understand the trade-offs between the cosmological sensitivity of samples obtainable under differing observational strategies, we carried out simulations to predict the number and distribution in redshift and magnitude of the set of SNe Ia detectable for survey of a given length and limiting magnitude set by the R-band exposure time. We adopt the methodology used in Tonry et al. (2003) to model the redshift-magnitude distribution of SNe Ia. In brief, we assume the supernovae luminosity function used in Li et al. (2001b), modeled as three distinct luminosity classes representing "normal" , over-luminous (1991T-like) and sub-luminous (1991bg-like) supernovae, each following a Gaussian distribution. This is then convolved with an estimated distribution of extinction due to dust in the supernova host galaxies (Hatano et al. 1998). We can then generate mock supernova samples for various possible survey implementations. For the purposes of survey optimization, it is sufficient to

---

[1] We consider here a prior on Ω_m alone, though in reality constraints from measurements of the matter power spectrum, baryon acoustic oscillations or cosmic microwave background produce constraints which have at least mild degeneracy with other cosmological parameters. This simple prior is sufficient for the survey optimization arguments presented here.
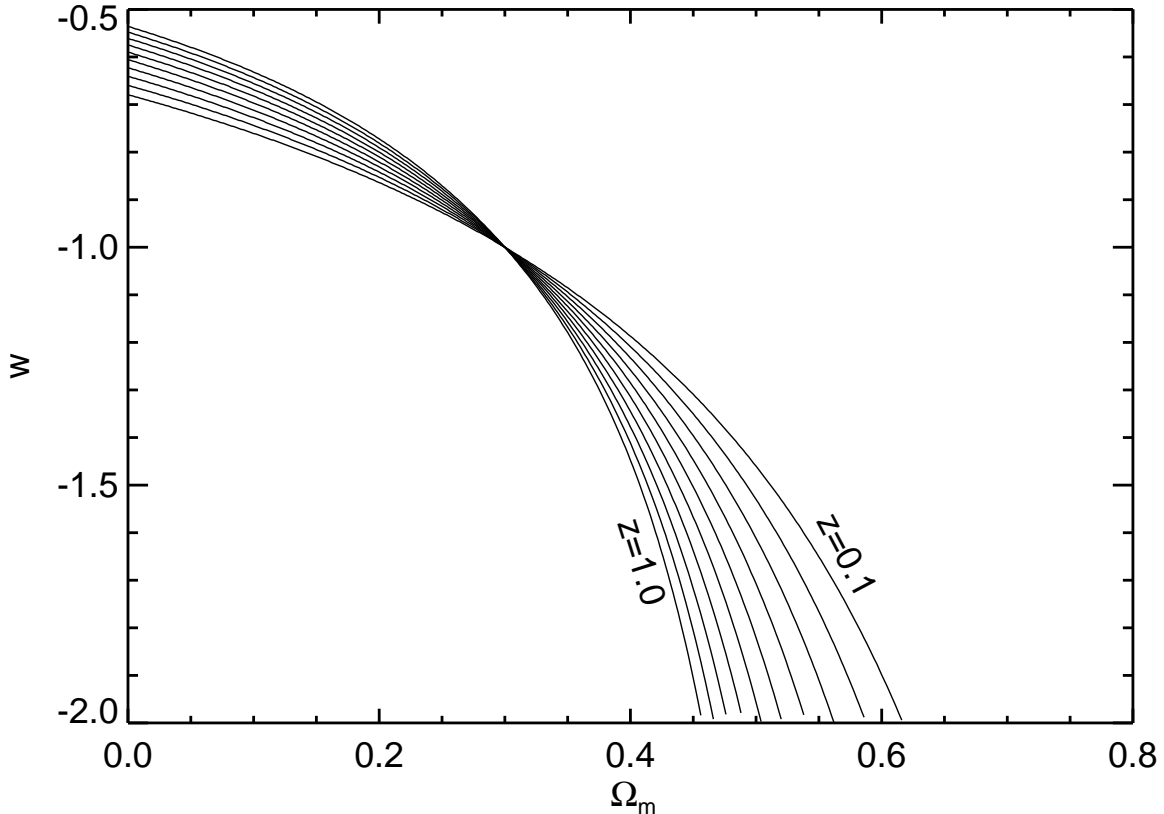
Fig. 2.— Curves in Ω_m and w for perfect measurements of distance at redshifts from 0.1 to 1.0, in steps of $\Delta z = 0.1$, for $\Omega_m = 0.3, \Omega_\Lambda = 0.7$.

restrict our considerations to flat cosmologies, neglecting degeneracies with $\Omega_{\mathrm{t}otal}$.

To estimate the acheivable cosmological constraints, we use an analytic description of how the uncertainty in distance modulus depends on redshift, as the typical signal-to-noise ratio of the photometry decreases at higher redshift, but the temporal sampling (in the SN rest frame) improves due to time dilation. The uncertainty in distance modulus is approximated by the expression:

$$\delta_\mu(z) = \frac{1.3}{SNR_{peak}} \times \sqrt{\frac{\Delta t_{obs}}{1+z}} \times \sqrt{\frac{N_{obs}}{N_{obs}-3}}, \tag{4}$$

where Δt_{obs} gives the time in days between observations, N_{obs} specifies the number of observations between -10 and +15 days (relative to maximum) in the SN rest frame, and the

$N_{obs} - 3$ term arises from three degrees of freedom in the fit of an SN light curve – time of maximum, luminosity at maximum and the width of the light curve.

This contribution to the distance uncertainty due to observational constraints is then summed in quadrature with the intrinsic dispersion in type Ia peak luminosities, taken conservatively to be 0.2 magnitudes. With the resulting mock Hubble diagrams, we then can predict the cosmological constraints obtainable for a given survey depth.

1.4. The ESSENCE Strategy

This generalized analysis can now be applied to our selected observational system, the Blanco 4m, in order to derive an optimal balance of photometric depth (or equivalently exposure time) and sky coverage given the range of conditions one might expect during a survey using a fixed amount of observing time. We assumed a five year survey with approximately 15 nights per year spread over three months each year. The results are shown in Figure 3. We find that the final achievable uncertainty in w is surprisingly insensitive to the survey depth, with the trade-off between the number of supernovae and the redshifts at which they are found roughly cancelling. There is a weak optimum at $t_R = 200$ seconds because very shallow surveys lose cosmological leverage as the redshift range probed decreases. After initially opting for a range of exposure times designed to match a range of redshift bins covering $z = 0.3 - -0.8$ in 2002, and finding that the efficiency at shorter exposure times was inadequate, we settled on exposure times of $t_R = 200$ seconds and $t_I = 400$ seconds as the baseline for the rest of the ESSENCE survey.

2. The ESSENCE Survey

2.1. Observations

Based on the survey strategy described above, the ESSENCE team submitted a proposal to the NOAO Survey program in 2002. We chose to propose a survey strategy to share time with the ongoing SuperMACHO survey, which uses only half nights on the Blanco telescope. ESSENCE was awarded 30 half nights per year for a five year program (recently extended to six), as well as additional calibration time on the CTIO 0.9m telescope together with some followup time on the WIYN 3.5m telescope. The ESSENCE time is generally scheduled during dark and grey time for three consecutive months, from October to December each year, although the timing of new moons sometimes moves the schedule into September or January. Each month, we observe every other night over a span of 20 days centered on new moon. This schedule leaves approximately ten bright nights each month with no light curve coverage.

2.1.1. The Instrument

ESSENCE survey data are taken using the MOSAIC II imaging camera, which consists of eight 2048x4096 pixel charge-coupled devices (CCDs) arranged in two rows of four, with gaps corresponding to approximately 50 pixels between rows and 35 pixels between columns. In the f/2.87 beam at prime focus, this yields a field of view of 0.6 degrees on a side for a total area of 0.36 square degrees on the sky. The CCDs are thinned back-illuminated silicon devices manufactured by SiTE with 15-um pixels. At the center of the focal plane, each pixel subtends 0.27 arc-seconds on a side, though the pixel scale varies quadratically as a function of radius due to optical aberrations, such that pixels at the corners of the camera subtend a smaller area on the sky by 8%.

The CCDs are read out in dual-channel mode, in which the chip is bisected in the long direction and read out in parallel through two separate amplifiers, for a read time of about 100 seconds. Because the amplifiers are not perfectly identical, we treat the sixteen resultant 1048x4096 "amplifier images" as independent data units in our data reduction. All ESSENCE observations are taken through the Atmospheric Dispersion Corrector (ADC), which is composed of two independently rotating prisms that compensate for variation in atmospheric refraction with airmass.

2.1.2. ESSENCE Fields

We selected fields that are equatorial, so that they can be accessed by telescopes in the northern and southern hemisphere for followup spectroscopy. The fields are spaced across the sky so that all observations may be taken at low airmass. We chose regions with low Milky Way extinction, for maximum visibility of these faint extra-galactic sources and to minimize systematic error incurred by correcting for extinction due to the Milky Way. Fields with contamination from bright stars, whose large footprint in the imaging data would reduce the effective search area, were avoided. Additional considerations in field selection included a preference for areas with minimal IR cirrus (based on IRAS maps), a preference for areas out of both the galactic and ecliptic planes, and a preference for fields which overlapped previous wide-field surveys (such as the Sloan Digital Sky Survey (SDSS), NOAO Deep Wide-Field Survey, and the Deep Lens Survey).

The first ESSENCE observations commenced on 2002 September 28. For this first year of operations, a set of 36 fields was defined. These fields were divided into two sets, which were then observed every other ESSENCE night, resulting in an cadence of every 4 nights on any particular field. This proved to be a challenging inaugural season for the project. The *El Niño* Pacific weather pattern was in effect, which produced heavy cloud cover much of time, resulting in either lost observing time or data of such poor quality that the detection of faint supernovae was often not possible. Also, the newly commissioned computing cluster experienced catastrophic failure shortly after data collection began, bringing real-time analysis of the data to a standstill for much of that observing campaign. On the night of November 9, the I-band filter sustained significant damage, resulting in a crack. This severely degraded the I band data quality in CCDs 1 and 2 (amplifiers 1-4), resulting in a diminished effective field of view for the rest of the season. This filter was replaced on May, 24, 2003.

As described below, many of the 2002 fields have not yet been repeated to provide template images to extract the supernova light curves. The complete analysis of the 2002 data will take place when these reference images are obtained. We provide summary information about the 15 spectroscopically confirmed Ia from this season in Table 3, we only present the light curves for four of these objects for which current reductions are of sufficient quality to merit use in the cosmological analysis in Wood-Vasey et al. (2007). The final ESSENCE supernova sample will include all of the 2002 objects.

Observations for the second year of ESSENCE began on September 28, 2003. In order to facilitate scheduling of follow-up observations with the Hubble Space Telescope (HST), which requires advance knowledge of the approximate location of the targets, it was necessary to cluster the search fields together into four groups. The new field set consisted of 32 fields, clustered spatially in sets of eight, such that they were within the pointing error box

of the HST. To the extent possible, fields from 2002 were used as the basis for the new fields. The fields were again divided into two separate sets, observed on alternating nights, providing for an observational cadence of every 4 nights for any given field. In table 1, we list the coordinates of the 32 search fields monitored by ESSENCE from 2003 onward. Results from the subset of nine ESSENCE supernovae observed with HST were presented in Krisciunas et al. (2005).

Table 1.   Coordinates of the centers of the ESSENCE search fields.

| Field Name	RA (J2000)	Dec (J2000)
waa1	23:29:52.92	-08:38:59.7
waa2	23:27:27.02	-08:38:59.7
waa3	23:25:01.12	-08:38:59.7
waa5	23:27:27.02	-09:14:59.7
waa6	23:25:01.12	-09:14:59.7
waa7	23:30:01.20	-09:44:55.9
waa8	23:27:27.02	-09:50:59.7
waa9	23:25:01.12	-09:50:59.7
wbb1	01:14:24.46	00:51:42.9
wbb3	01:09:36.40	00:46:43.3
wbb4	01:14:24.46	00:15:42.9
wbb5	01:12:00.46	00:15:42.9
wbb6	01:09:00.16	+00:10:43.3
wbb7	01:14:24.46	-00:20:17.1
wbb8	01:12:00.46	-00:20:17.1
wbb9	01:09:36.40	-00:25:16.7
wcc1	02:10:00.90	-03:45:00.0
wcc2	02:07:40.60	-03:45:00.0
wcc3	02:05:20.30	-03:45:00.0
wcc4	02:10:01.20	-04:20:00.0
wcc5	02:07:40.80	-04:20:00.0
wcc7	02:10:01.55	-04:55:00.0
wcc8	02:07:41.03	-04:55:00.0
wcc9	02:05:20.52	-04:55:00.0
wdd2	02:31:00.25	-07:48:17.3
wdd3	02:28:36.25	-07:48:17.3
wdd4	02:34:30.35	-08:19:18.2
wdd5	02:31:00.25	-08:24:17.3
wdd6	02:28:36.25	-08:24:17.3
wdd7	02:33:24.25	-08:55:18.2
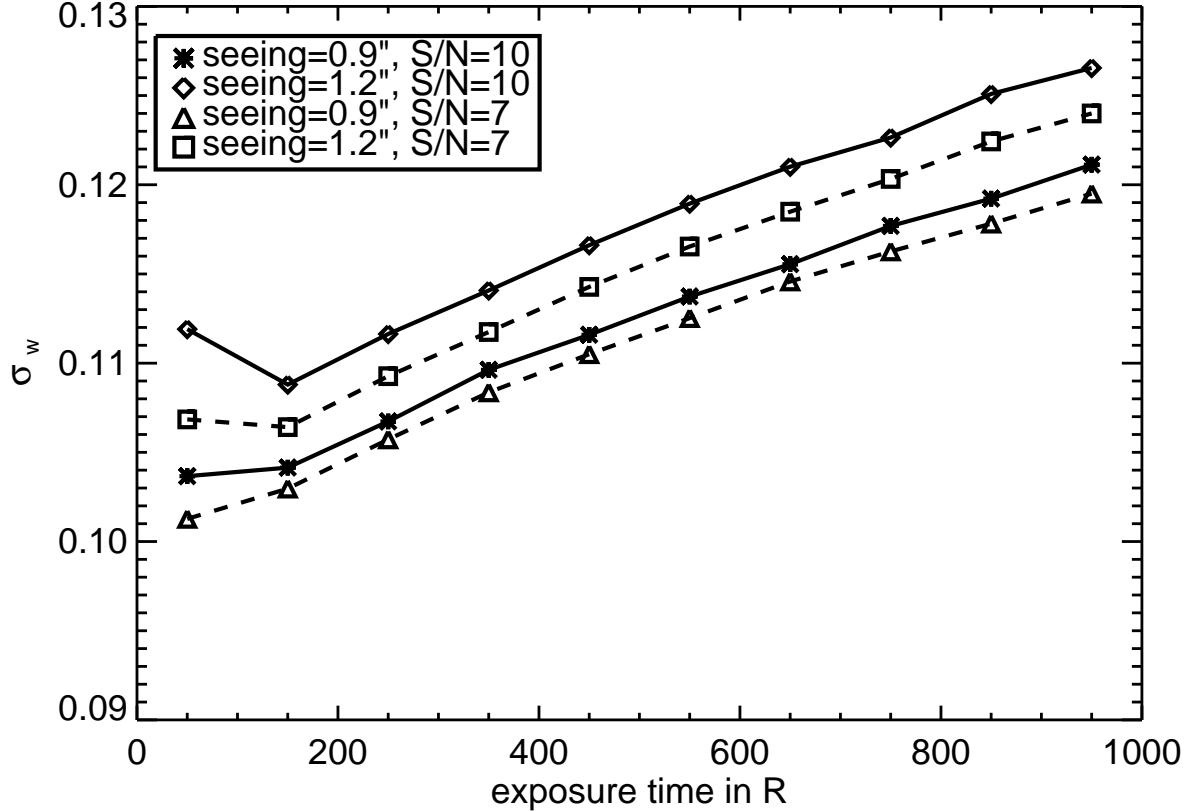
Fig. 3.— Estimated final uncertainty in w for a 5 year ESSENCE survey when combined with $\Omega_M = 0.3 \pm 0.04$ constraints from Tegmark et al. (2004), as a function of R-band exposure time for the survey. A range of typical survey seeing conditions and detection thresholds was chosen. Here we show the effects of mean seeing, which degrades the precision of the photometry, and the signal-to-noise threshold at which we are able to detect supernovae in our data, which affects the total number observable.

Table 1—Continued

Field Name	RA (J2000)	Dec (J2000)
wdd8	02:31:00.25	-09:00:17.3
wdd9	02:28:36.25	-09:00:17.3

Note. — For reference, the CTIO 4-m MO-SAIC II detector has a field of view of 0.36 square degrees.

Weather and observing conditions for 2003 were greatly improved over 2002, though still somewhat sub-standard for typical conditions at Cerro Tololo. Unfortunately, one of the MOSAIC CCDs (containing amplifiers 5 and 6) failed shortly before the observations began, resulting in a 12.5% loss in efficiency. The failed CCD was replaced before our 2004 observing season, allowing us to recover the lost efficiency from then on. For the third year and fourth years of ESSENCE, we maintained the same set of fields as in 2003 and the MOSAIC imager was stable. The supernovae yields for each of the four years of the survey are summarized in Table 2. The ESSENCE search is successful and our program finds roughly twice as many objects with SN-like light curves than we can follow up spectroscopically each year.

Table 2.   Summary of the supernova yields from the first four years of ESSENCE observations.

Year	Spectroscopically Confirmed Supernovae	Type Ia Supernovae
2002	15	15
2003	37	33
2004	41	26
2005	46	28

2.2. Image Analysis Pipeline

The ESSENCE program requires immediate reduction of each night's data (typically ~ 4 GB each night), so it is more convenient to base operations at the NOAO/CTIO offices in the nearby city of La Serena, rather than directly at the telescope. Therefore, ESSENCE team members carry out observations remotely from a terminal at La Serena, communicating with telescope operators on the mountain via a video-conferencing link. Incoming data may be viewed by connecting directly to computers at the telescope, which allows real-time quality control, while in parallel the data are immediately transferred to computing hardware in La Serena via an internet link.

The analysis of ground-based imaging data is a complicated multi-stage procedure, involving the removal of instrumental artifacts, calibration of the data and measurements of the fluxes from the objects of interest. The particular demands of a supernova survey place more demanding constraints on the image analysis software.

First, the objects of interest are transient and appear in the data masked by the background flux from their host galaxy. Past experience has shown that the most reliable way to find these objects is via image subtraction (Norgaard-Nielsen et al. 1989; Perlmutter et al. 1995; Schmidt et al. 1998). For each new image, an archival "template" frame from a previous epoch is subtracted pixel-by-pixel to remove constant sources, such as galaxies, to reveal the supernovae. Image subtraction software is not part of standard analysis packages and we have invested significant effort in developing robust and reliable methods necessary for our project.

Second, supernovae must be detected in *real time*. While it is a part of our search strategy to revisit each field and build up a time series of photometric measurements of all objects, we rely on follow-up spectroscopic observations to verify the identity of candidate transients as type Ia supernovae and to establish their redshifts. Because supernovae at the distances that give cosmological leverage are faint ($m \sim 22$) even at maximum light, it is preferable to observe them near maximum light. Type Ia supernovae rise to maximum light roughly 20 days after explosion in their rest frame (Riess et al. 1999a; Conley et al. 2006; Garg et al. 2006), and while time dilation stretches the rise of a supernova by a factor of $1 + z$, a prompt detection allows us to schedule the spectroscopic observations into the available time. This real-time component adds a significant demand on the analysis of the survey data: the data must be processed automatically and reliably, in bulk, each night of the survey.

Finally, supernovae are rare events. We expect roughly one supernova per MOSAIC field per month. Each MOSAIC field consists of $4096 \times 2048 \times 8 = 67,000,000$ pixels, and

we must be able to reliably determine the ∼dozen pixels among those that contain signal, often only marginally above background noise, from a *bona fide* type Ia supernova. [2]

We have developed a data pipeline that meets these demands, accepting raw images directly from the telescope and automatically producing lists of candidate objects only hours later. Floating point operations are carried out by a variety of programs, either drawn from publicly available astronomical software packages, such as IRAF[3] , or written by us (generally in C). These are tied together by a suite of Perl scripts, which handle process management and bookkeeping. Functionally, there are two separate piplines. The first of these ("mscpipe") performs tasks relevant for full MOSAIC images and as output divides each single MOSAIC field into sixteen 1k x 4k pixel images corresponding to each CCD amplifier. From this point onward, the "amplifier-images" are processed through "photpipe" and each amplifier is effectively treated as an independent detector. We will refer to a single MOSAIC exposure as a MOSAIC field and the subdivided images as subfields. Below we provide a brief description of the data processing, focusing in particular on those stages that alter the data in ways significant for the analysis.

2.2.1. Crosstalk correction

Pairs of CCDs in the MOSAIC II imager are read out through single electronics controllers, which, for some combinations of CCDs, results in low-level cross-talk between the signals from different chips. The resulting effect is the appearance of "ghosts" in one subfield of bright objects appearing in another subfield. Fortunately, this effect is small in magnitude, on the order of 0.1%, and deterministic. The first stage of the *mscpipe* pipeline uses the most recent values of these cross-talk coefficients measured by the observatory staff and subtracts these electronic artifacts from the affected portions of the MOSAIC field, using the *xtalk* task from the *mscred* package for IRAF.

---

[2]If there are roughly 10 needles to a gram and a typical haystack weighs 1000 kilograms, then finding the part per 10^7 supernova pixels in one frame is truly like finding a needle in a haystack. And we need to sift 20 per night!

[3]IRAF is distributed by the National Optical Astronomy Observatory, which is operated by AURA under cooperative agreement with the NSF.

2.2.2. Astrometric calibration

The transformation from pixel to sky coordinates is dominated by distortions due to the optical system of the telescope that change only slightly over long periods of time and generally take the form of a polynomial in radius. Once the terms of this distortion function are known, the astrometric calibration of any particular image reduces to determining accurately the center of the distortion in that field, essentially an offset in x and y and a rotation. This is accomplished via the IRAF task *msccmatch* from the *mscred* package, which matches objects in the image to an existing catalog of the field with precise astrometry. The current standard for astrometry is the USNO CCD Astrograph Catalog 2 (UCAC, Zacharias et al. (2004)) , which covers all fields observed by ESSENCE. However, since ESSENCE is a significantly deeper survey, the Sloan Digital Sky Survey (SDSS, York et al. (2000)) provides a better photometric overlap. We use the SDSS (which itself is tied to UCAC) in the fields for which SDSS has imaging data ($\sim 73\%$ of ESSENCE fields), and default to UCAC when there is no SDSS data.

When the supernovae are faint, their location in an image is poorly constrained, and we must rely on the astrometric solution to tell us precisely where to measure the flux. Errors in positioning the PSF produce an underestimate the object's flux. Therefore, accurate *relative* astrometric calibration is essential to measuring supernova flux at low signal-to-noise, since what matters is that we are able to map pixels from invidividual images to some consistent coordinate system. To this end, we generate astrometric catalogs from our own data, which are themselves calibrated to either SDSS or UCAC. All subsequent ESSENCE images are then registered to these internally generated catalogs.

The astrometric solution is also used to "warp" each image to a common pixel coordinate system, so that reference images can be subtracted from them. This is accomplished using the SWarp (Bertin et al. 2002) software package, using a Lanczos windowed sinc function to resample the pixels onto the new coordinate system.

2.2.3. Flatfielding

In order to obtain consistent flux measurements across the plane of MOSAIC imager, we must normalize the response of all the pixels. This flat fielding is achieved in three steps. First, at the beginning of each night, a screen inside the telescope dome is illuminated and observed with the MOSAIC. These high signal-to-noise flatfields enable us to accurately correct for pixel-to-pixel variations and other imperfections in the optical system, but introduces large-scale variations (e.g. gradients due to non-uniform illumination of the flat-field screen).

The second step is to combine all of the data from a night's observations. By masking all astronomical sources and combining with a median statistic, an image of the illumination of the focal plane due to the night sky is created. This "illumination correction" is also applied to the data, removing gradients of $\sim 1\%$ across a CCD. Finally, we use the average difference in sky level between each ccd to further regularize the overall flux scaling, a 1% correction to the dome flats.

2.2.4. Photometric calibration

Flat-fielded and SWarped images are then analyzed with the DoPHOT photometry package (Schechter et al. 1993) to identify and measure sources. This instrumental photometry is then calibrated against a catalog of objects with known magnitudes, to determine the photometric zeropoint for the image. Further discussion of photometric calibrations follows in Section 3.

2.2.5. Image subtraction

Each image is then differenced against a reference image. This suppresses all constant sources of flux and reveals transients such as new supernovae. To subtract two images taken under different atmospheric conditions on different nights, we must correct for seeing variations. Our image subtraction software uses the algorithm devised by Alard and Lupton (Alard & Lupton 1998; Alard 2000) to determine and apply a convolution that matches the point-spread functions of the two images prior to subtraction. Improvements to the basic method have produced a process that automatically, robustly, and reliably produces clean subtractions in our data.

2.2.6. Difference image object detection

Object detection in the subtracted images is done with a modified version of DOPHOT. Resampling and convolution of the images correlates flux between pixels, so we have modified the image registration and subtraction software to propagate noise maps that track these correlations. These are then used to evaluate the significance of objects detected in the difference image.

2.3. Candidate selection

Each observation of a single ESSENCE field yields hundreds of objects detected above some significance threshold in the subtracted images. These must be culled to produce a small set of objects that are very likely to be type Ia supernovae and merit spectroscopic observation on large telescopes. We first apply a series of software cuts, which include

- requiring that the object has the same PSF as stars in the original, unsubtracted image,

- vetoing detections with significant amounts of pixels with negative flux, to guard against subtraction residuals, such as dipoles resulting from slight image misalignment,

- vetoing variable sources identified in previous data (variable stars, active galactic nuclei) and

- requiring coincident detections in more than one passband or on subsequent nights, to reject asteroids (typically, two detections at signal-to-noise ratio > 5 within a five day window).

While the above rules eliminate many of the false positives, we ultimately rely on human inspection to reject the small fraction of contaminants that evade these filters. Common problems include insufficient masking of pixels from bright stars, subtraction artifacts, and variable objects that have not varied significantly in previous ESSENCE data.

We also perform light curve fits to assess whether each object is consistent with the known behavior of SN Ia. Preliminary fits of the initial R and I photometry are compared with light curve templates of a type Ia SN at z=0 in B and V filters (which are a good match for SN Ia at z~0.4-0.5). The template light curve is representative of a normal type Ia SN with $\Delta_{m15} = 1.1$ mag, or stretch=1, and was contructed from well-sampled light curves of low-z supernovae (Prieto et al. 2006). Using a chi-squared minimization, we determine the the best fit values for time of B maximum, observed R and I magnitudes at maximum, and stretch. We chose to use stretch here because it parametrizes in a simple way the variety of light curve shapes of SNe Ia (Goldhaber et al. 2001). Using the R and I magnitudes at maximum and the stretch obtained from the fit, we can now estimate a photometric redshift assuming that the candidate is a type Ia SN. A standard ΛCDM with $\Omega_M = 0.3$, $\Omega_\Lambda = 0.7$ is used and no host galaxy reddening is considered in these fits.

A summary of the data for each candidate object is presented on a web page for human inspection. We reject detections resulting from subtraction artifacts by looking at image "stamps" at the position of the supernova. The light curves from the preliminary photometry

enable us to reject objects that clearly have the wrong light curve shape, color, and brightness for a supernova in the estimated redshift range.

Because our spectroscopy resources are limited, we have to make choices to observe the most promising targets. We select against objects right at the centers of galaxies both because past experience has shown that these are frequently active galactic nuclei and because contamination from the galaxy often makes it impossible to positively identify the supernova in a spectrum. To avoid these problems, we select against candidates that are superposed on point-like sources in the central pixel (0.27") of the template image. We know that the SN Ia in galaxy centers have a broader distribution in apparent luminosity from SN Ia generally (Jha et al. 2007), but we do not expect any significant cosmological bias from this selection criterion.

The objects that pass the above selection procedure are then sent to team members for spectroscopic observation. Because spectroscopy time is limited and scheduled in advance, we are forced to prioritize those objects that look most promising based on the data available at the time. Our survey is spectroscopy-limited: at the end of each observing campaign, many objects remain that have Ia-like light curves, but for which we were unable to obtain follow-up spectroscopy. Nevertheless, we successfully detect and confirm new supernovae at a rate of roughly one new object per night of 4m observing.

3. Spectroscopy

3.1. Observations

Follow-up spectroscopic observations of ESSENCE targets are performed at a wide variety of ground-based telescopes: the 10-m Keck I (+LRIS; Oke et al. 1995) and II (+ESI, Sheinis et al. 2002; +DEIMOS, Faber et al. 2003) telescopes; the 8-m VLT (+FORS1; Appenzeller et al. 1998), Gemini North and South (+GMOS; Hook et al. 2003) telescopes; the 6.5-m Magellan Baade (+IMACS; Dressler 2004) and Clay (+LDSS2; Mulchaey 2001), MMT (+BlueChannel; Schmidt et al. 1989) telescopes. One target (d100.waa7_16; see Matheson et al. 2005) was confirmed as a Type Ia supernova using the FAST spectrograph (Fabricant et al. 1998) on the 1.5-m Tillinghast telescope at the F. L. Whipple Observatory (FLWO). The useful sample of supernovae from the ESSENCE program is limited by our ability to identify SNe Ia spectroscopically.

Standard CCD processing and spectrum extraction are done with standard IRAF routines. Except for the VLT data, all the spectra are extracted using the optimal algorithm of Horne (1986). For the VLT data, we apply a novel extraction method based on two-channel Richardson-Lucy restoration (Blondin et al. 2005) to minimize contamination of the supernova spectrum by underlying galaxy light. The spectra are wavelength calibrated using calibration-lamp spectra (usually HeNeAr). For the flux calibration we use both standard IRAF routines and our own IDL procedures, which include the removal of telluric lines using the well-exposed continua of the spectrophotometric standard stars (Wade & Horne 1988; Matheson et al. 2000b).

3.2. Supernova classification and redshift determination

Supernovae are classified according to their early-time spectra (see Filippenko 1997, for a review). The distinctive spectroscopic signature of a Type Ia supernova near maximum light is a deep absorption feature due to Si II $\lambda6355$, blueshifted by ~ 10000 km s^{-1}. Their spectra are further characterized by the absence of hydrogen and helium lines, although hydrogen has been detected in the spectrum of the Type Ia supernova SN 2002ic (Hamuy et al. 2003; Wood-Vasey et al. 2004) (Benetti et al. (2006) classify this object as an Type Ib/c). Spectra of Type Ib supernovae are characterized by a weaker Si II $\lambda6355$ absorption, and by the presence of lines of He I. Spectra of Type Ic supernovae are devoid of He I lines and display only a weak Si II $\lambda6355$ absorption. Thus, in principle, SNe Ib/c are readily distinguishable from SNe Ia.

At high ($z \gtrsim 0.4$) redshifts, however, the defining Si II $\lambda6355$ feature in SNe Ia is redshifted out of the optical range of most of the spectrographs we use, so features blueward of this must be used to establish the type. The most prominent of these, the Ca II H&K $\lambda\lambda3934,3968$ doublet, is also present in SNe Ib/c and does not discriminate between the various supernova types. Instead, the identification of SNe Ia relies on weaker features (e.g., Si II $\lambda4130$, Mg II $\lambda4481$, Fe II $\lambda4555$, Si III $\lambda4560$, S II $\lambda4816$, and Si II $\lambda5051$).

While the above gives the general defining features of Ia spectra, in practice, identfying SNe Ia can be difficult in low signal-to-noise spectra, particular when trying to discriminate between SNe Ia and SNe Ib/c. In addition, we would like to establish objective and reproducible criteria for classifying objects, rather than relying on subjective assessments of noisy data. Therefore, we have developed an algorithm (SuperNova IDentification, or SNID; Blondin & Tonry 2007) also used by Matheson et al. (2005), which we use here to establish our final SN Ia sample. This algorithm cross-correlates an input spectrum with a library of supernova spectra, without attempting to directly identify specific features, and a redshift is determined based on the shift in wavelength that maximizes the correlation. The spectral database currently spans all supernova types and covers a wide range of ages, containing 796 spectra of 64 SNe Ia (including spectra of 1991T-like and 1991bg-like objects), 288 spectra of 17 SNe Ib/c, and 353 spectra of 10 SNe II. We also include spectra of galaxies, AGNs, and stars to identify spectra that are not consistent with a supernova (see also Matheson et al. 2005). The results of the SNID analysis are shown in Table 3.

The correlation redshift is valid when templates of the correct supernova type are used. We also use SNID to determine the supernova type, by computing the absolute fraction of "good" correlations that correspond to supernovae of different types. The supernova types/subtypes in the SNID spectral database are: Ia/Ia-norm, Ia-pec, Ia-91t, Ia-91bg; Ib/Ib-norm, Ib-pec, IIb; Ic/Ic-norm, Ic-pec, Ic-broad; II/II-norm, II-pec, IIL, IIn, IIP, IIb. "Norm" and "pec" subtypes are used to identify the spectroscopically "normal" and "peculiar" supernovae of a given type, respectively. For type Ia supernovae, "91t" and "91bg" indicates spectra that resemble those of the overluminous SN 1991T and the underluminous SN 1991bg, respectively. The spectra that correspond to the "Ia-pec" category in this case are those of SNe 2000cx (Li et al. 2001a; Candia et al. 2003) and 2002cx (Li et al. 2003). For type Ic supernovae, 'Ic-broad' is used to identify broad-lined SNe Ic, (often referred to as "hypernovae" in the literature), some of which are associated with Gamma-Ray Bursts. The notation used for the type II subtypes are commonly used in the literature. Note that type IIb supernovae (whose spectra evolve from a type II to a type Ib, as, e.g., in SN 1993J– see Matheson et al. 2000a) are included both in the "Ib" and "II" types.

If the redshift of the supernova host galaxy can be measured using narrow emission or

absorption lines, we force SNID to look for correlations at the galaxy redshift (± 0.03) to determine the supernova type/subtype; otherwise the redshift is left as a free parameter. We assert a supernova to be of a given type (i.e., Ia, Ib, Ic, II, see Table 3, column 3) when the absolute fraction of "good" correlations that correspond to this type exceeds 50%. In addition, we require the best-match supernova template to be of the same type. We determine the supernova subtype by requiring that the absolute fraction of "good" correlations that correspond to this subtype exceeds 50%, *and* that it corresponds to the previously-determined type. We also require that the best-match supernova template is of the same subtype.

The requirement that an object must have a correlation fraction above 50% is motivated by the desire to have a quantative figure of merit that determines when the spectral information is strong enough to make a positive identification. Out of all the spectra that were considered to be those of possible supernovae, 28 did not meet the above criteria for a positive classification (see Table 3). Assessing the likelihood that a spectrum matches that of particular known object more closely than others is a challenging statistical problem, especially in the presence of intrinsic and only partially understood variance in the populations of supernovae. See Blondin & Tonry (2007) for a detailed discussion of ongoing work to better understand these issues.

The redshift is then determined from the supernova spectrum alone in a second SNID run by considering correlations with templates of the determined type and subtype. No *a priori* information on redshift is used in this second run. The supernova redshift is reported as the median redshift of all "good" correlations, and the redshift error as the standard deviation of these same redshifts. When there is only one "good" correlation for an input spectrum (objects d087, h311, and p524 in Table 3), we quote the redshift as that of the best-match template and the associated error as the formal redshift error for that template (see Blondin & Tonry 2007). We only report a SN redshift when a secure type is determined. In Matheson et al. (2005) we found an excellent agreement between the SNID correlation redshift and the redshift of the supernova host galaxy when it is known from other methods. Figure 4 again shows that the SNID redshifts agree well with the galaxy redshifts, with a typical uncertainty $\lesssim 0.01$ in the redshift range $[0.1 - 0.8]$. Figure 5 shows the redshift distribution of the spectroscopically confirmed SNe Ia from the first four years of ESSENCE.

Table 3. Types and Redshifts of ESSENCE Supernovae.

IAUC ID	RA [J2000]	Dec [J2000]	ESSENCE ID	Type	Subtype	%Subtype	%Ia	%Ib/c	%II	z_{GAL}	z_{SNID}	σ_z
2002iu	00:13:33.10	-10:13:09.92	b003	Ia	Ia-norm	74.2	100.0	0.0	0.0	—	0.115	0.006
2002iv	02:19:16.11	-07:44:06.72	b004	Ia	Ia-91t	64.4	98.3	1.7	0.0	0.231	0.226	0.003
2002jq	23:35:57.96	-10:05:56.88	b008	Ia	Ia-norm	65.1	81.4	11.6	7.0	—	0.474	0.004
2002iy	02:30:40.00	-08:11:40.50	b010	Ia	Ia-norm	73.6	82.4	17.6	0.0	0.587	0.590	0.006
2002iz	02:31:20.73	-08:36:13.12	b013	Ia	Ia-norm	85.8	98.6	1.4	0.0	0.428	0.426	0.004
2002ja	23:30:09.66	-09:35:01.75	b016	Ia	Ia-norm	100.0	100.0	0.0	0.0	—	0.329	0.003
2002jb	23:29:44.14	-09:36:34.25	b017	Ia	Ia-norm	75.5	100.0	0.0	0.0	—	0.258	0.007
2002jr	02:04:41.03	-05:09:40.73	b020	Ia	Ia-norm	81.8	100.0	0.0	0.0	—	0.425	0.003
2002jc	02:07:27.28	-03:50:20.73	b022	Ia	Ia-norm	55.7	65.7	24.3	10.0	—	0.540	0.008
2002js	02:20:35.39	-09:34:43.90	b023	Ia	Ia-norm	90.9	100.0	0.0	0.0	—	0.550	0.007
2002jd	00:28:38.39	+00:40:29.29	b027	Ia	Ia-norm	79.2	96.6	3.4	0.0	—	0.318	0.005
2002jt	00:13:36.70	-10:08:24.00	c003	Ia	—[a]	—	100.0	0.0	0.0	—	0.382	0.002
2002ju	02:20:11.00	-09:04:37.50	c012	Ia	Ia-norm	72.6	100.0	0.0	0.0	0.348	0.350	0.006
2002jw	02:30:00.52	-08:36:22.41	c015	Ia	Ia-norm	76.6	100.0	0.0	0.0	0.357	0.362	0.008
—	00:28:03.16	+00:37:50.43	c023	Ia	Ia-norm	100.0	100.0	0.0	0.0	0.399	0.400	0.009
2003jo	23:25:24.03	-09:26:00.63	d033	Ia	Ia-norm	76.0	96.0	4.0	0.0	0.524	0.531	0.008
2003jj	01:07:58.52	+00:03:01.89	d058	Ia	Ia-norm	85.0	95.0	5.0	0.0	0.583	0.583	0.009
2003jn	02:29:21.21	-09:02:15.57	d083	Ia	Ia-91t	56.5	100.0	0.0	0.0	—	0.333	0.002
2003jm	02:28:50.93	-09:09:58.14	d084	Ia	Ia-norm	68.6	100.0	0.0	0.0	0.522	0.519	0.007
2003jv	23:27:58.22	-08:57:11.82	d085	Ia	Ia-91t	100.0	100.0	0.0	0.0	0.405	0.401	0.001
2003ju	23:27:01.71	-09:24:04.49	d086	Ia	Ia-norm	87.5	100.0	0.0	0.0	—	0.205	0.003
2003jr	01:11:06.23	+00:13:44.21	d087	Ia	Ia-norm	100.0	100.0	0.0	0.0	0.340	0.337[b]	0.009
2003jl	02:28:28.56	-08:08:44.74	d089	Ia	Ia-norm	92.3	100.0	0.0	0.0	0.429	0.436	0.006
2003js	02:29:52.15	-08:32:28.09	d093	Ia	Ia-91t	63.1	93.4	6.6	0.0	0.363	0.360	0.004
2003jt	02:31:54.60	-08:35:48.43	d097	Ia	Ia-norm	95.7	100.0	0.0	0.0	—	0.436	0.008
2003ji	02:07:54.84	-03:28:28.40	d099	Ia	Ia-norm	77.5	96.9	2.0	1.0	—	0.211	0.003
2003jq	23:30:51.19	-09:28:33.95	d100	Ia	Ia-norm	67.8	98.3	1.7	0.0	—	0.156	0.003
2003jw	02:31:06.84	-08:45:36.51	d117	Ia	Ia-norm	84.6	100.0	0.0	0.0	0.296	0.309	0.006
2003jy	02:10:53.98	-04:25:49.76	d149	Ia	Ia-norm	100.0	100.0	0.0	0.0	0.339	0.342	0.006
2003kk	23:25:36.06	-09:31:44.70	e020	Ia	Ia-norm	88.4	100.0	0.0	0.0	0.164	0.159	0.007
2003kl	01:09:48.80	+01:00:05.58	e029	Ia	Ia-norm	74.7	100.0	0.0	0.0	0.335	0.332	0.008
2003km	02:30:01.00	-09:04:35.89	e108	Ia	Ia-norm	100.0	100.0	0.0	0.0	—	0.469	0.005
2003kn	02:09:15.55	-03:35:41.38	e132	Ia	Ia-norm	76.3	100.0	0.0	0.0	0.244	0.239	0.006
2003ko	02:11:06.48	-03:47:56.09	e136	Ia	Ia-norm	85.1	99.2	0.8	0.0	0.360	0.352	0.007

Table 3—Continued

IAUC ID	RA [J2000]	Dec [J2000]	ESSENCE ID	Type	Subtype	%Subtype	%Ia	%Ib/c	%II	z_{GAL}	z_{SNID}	σ_z
2003kt	02:33:47.01	-08:36:22.09	e138	Ia	Ia-norm	100.0	100.0	0.0	0.0	—	0.612	0.009
2003kq	02:31:04.09	-08:10:56.64	e140	Ia	Ia-norm	100.0	100.0	0.0	0.0	0.606	0.631	0.007
2003kp	02:31:02.64	-08:39:50.81	e147	Ia	Ia-norm	100.0	100.0	0.0	0.0	—	0.645	0.010
2003kr	02:31:20.96	-08:36:14.16	e148	Ia	Ia-norm	100.0	100.0	0.0	0.0	0.427	0.429	0.006
2003ks	02:31:34.54	-08:36:46.41	e149	Ia	Ia-norm	81.4	98.6	1.4	0.0	—	0.497	0.006
2003ku[c]	01:08:36.25	-00:33:20.78	e315	—	—	—	—	—	—	—	—	—
2003kv[c]	02:09:42.52	-03:46:48.58	e531	—	—	—	—	—	—	—	—	—
2003lh	02:10:19.51	-04:59:32.30	f011	Ia	Ia-norm	100.0	100.0	0.0	0.0	—	0.539	0.004
2003le	01:08:08.73	+00:27:09.74	f041	Ia	Ia-norm	68.8	100.0	0.0	0.0	—	0.561	0.006
2003lf	01:08:49.81	-00:44:13.49	f076	Ia	Ia-norm	82.2	100.0	0.0	0.0	—	0.410	0.007
2003lm	23:24:25.51	-08:45:51.11	f096	Ia	Ia-norm	88.5	100.0	0.0	0.0	0.408	0.412	0.006
2003ll	02:35:41.19	-08:06:29.55	f216	Ia	Ia-norm	75.0	100.0	0.0	0.0	0.596	0.599	0.005
2003lk[d]	02:11:12.82	-04:13:52.11	f221	—	—	—	33.3	66.7	0.0	0.442	—	—
2003ln	23:30:27.15	-08:35:46.98	f231	Ia	Ia-norm	100.0	100.0	0.0	0.0	—	0.619	0.008
2003lj	01:12:10.03	+00:19:51.29	f235	Ia	Ia-norm	87.8	100.0	0.0	0.0	0.417	0.422	0.007
2003li	02:27:47.29	-07:33:46.16	f244	Ia	Ia-norm	100.0	100.0	0.0	0.0	0.544	0.540	0.004
—[d]	02:27:26.51	-08:42:24.88	f301	—	—	50.0	75.0	14.3	10.7	—	—	—
—	02:29:22.39	-08:37:38.38	f308	Ia	Ia-norm	66.7	100.0	0.0	0.0	—	0.394	0.009
2004fi[c]	23:29:45.35	-08:54:36.34	g001	—	—	—	—	—	—	0.265	—	—
2004fh	23:28:27.20	-08:36:55.17	g005	Ia	Ia-norm	72.9	100.0	0.0	0.0	—	0.218	0.007
2004fj	01:09:51.07	+00:27:20.95	g043	II	IIP	100.0	0.0	0.0	100.0	0.187	0.193	0.002
2004fn	23:30:20.12	-09:58:30.67	g050	Ia	Ia-norm	100.0	100.0	0.0	0.0	0.605	0.633	0.006
2004fm	23:26:58.14	-09:37:19.45	g052	Ia	Ia-norm	80.0	100.0	0.0	0.0	—	0.383	0.008
2004fl[c]	23:26:57.92	-09:37:19.11	g053	—	—	—	—	—	—	—	—	—
2004fk	01:13:35.84	-00:09:27.56	g055	Ia	Ia-norm	79.3	100.0	0.0	0.0	0.296	0.302	0.006
—	23:27:37.16	-09:35:20.96	g097	Ia	Ia-norm	62.8	81.4	18.6	0.0	0.343	0.340	0.004
2004fo	01:13:28.97	+00:35:16.26	g120	Ia	Ia-norm	94.7	100.0	0.0	0.0	—	0.510	0.009
—	02:09:49.63	-04:10:55.07	g133	Ia	Ia-norm	75.0	98.8	0.0	1.2	—	0.421	0.003
—	23:28:37.70	-08:45:04.01	g142	Ia	Ia-norm	58.2	98.5	1.5	0.0	0.404	0.399	0.003
2004fq[c]	23:27:45.64	-08:31:12.77	g151	—	—	—	—	—	—	0.146	—	—
2004fs	02:31:19.95	-08:49:21.67	g160	Ia	Ia-norm	89.5	100.0	0.0	0.0	—	0.493	0.003
2004fr[c]	02:28:43.77	-08:54:24.05	g166	—	—	—	—	—	—	0.202	—	—
2004ft[c]	02:33:32.63	-08:09:34.10	g199	—	—	—	—	—	—	—	—	—
—[c]	23:27:15.69	-09:27:59.76	g225	—	—	—	—	—	—	—	—	—

Table 3—Continued

IAUC ID	RA [J2000]	Dec [J2000]	ESSENCE ID	Type	Subtype	%Subtype	%Ia	%Ib/c	%II	$z_{\rm GAL}$	$z_{\rm SNID}$	σ_z
— [d]	01:11:56.31	+00:07:27.71	g230	—	—	—	50.0	0.0	50.0	0.392	—	—
—	23:30:41.83	-08:34:10.98	g240	Ia	Ia-norm	86.7	100.0	0.0	0.0	—	0.687	0.005
— [c]	02:04:27.01	-03:35:43.72	g276	—	—	—	—	—	—	0.244	—	—
2004ha	02:04:27.01	-04:52:46.03	h283	Ia	Ia-norm	85.7	100.0	0.0	0.0	—	0.502	0.008
—	02:31:40.67	-08:49:03.35	h300	Ia	Ia-norm	100.0	100.0	0.0	0.0	—	0.687	0.012
2004hc	23:24:32.67	-08:41:03.55	h311	Ia	Ia-norm	100.0	100.0	0.0	0.0	—	0.741[b]	0.011
2004hd	02:08:48.21	-04:26:10.42	h319	Ia	Ia-norm	100.0	100.0	0.0	0.0	0.490	0.495	0.004
2004he	02:29:48.79	-08:20:45.94	h323	Ia	Ia-norm	100.0	100.0	0.0	0.0	0.598	0.603	0.006
2004hf	02:32:00.14	-08:42:23.89	h342	Ia	Ia-norm	100.0	100.0	0.0	0.0	—	0.421	0.002
2004hg[c]	02:34:55.19	-08:30:43.64	h345	—	—	—	—	—	—	—	—	—
2004hi	02:08:38.84	-05:08:11.79	h359	Ia	Ia-norm	46.8	68.1	31.9	0.0	—	0.348	0.004
2004hh	02:06:25.02	-04:38:04.09	h363	Ia	Ia-norm	69.0	97.7	0.0	2.3	—	0.213	0.006
2004hj	02:29:41.94	-08:43:49.42	h364	Ia	Ia-norm	100.0	100.0	0.0	0.0	—	0.344	0.007
2004hk[c]	23:27:04.39	-08:38:45.11	k396	—	—	—	—	—	—	—	—	—
—	23:26:11.77	-08:50:17.50	k411	Ia	Ia-norm	78.6	85.7	14.3	0.0	—	0.564	0.006
2004hl	01:13:38.17	-00:27:39.03	k425	Ia	Ia-norm	82.9	97.1	0.0	2.9	0.270	0.274	0.003
2004hm	02:28:03.12	-07:42:29.70	k429	Ia	Ia-norm	66.7	100.0	0.0	0.0	0.172	0.181	0.008
2004hn	01:13:32.39	+00:37:15.38	k430	Ia	Ia-norm	100.0	100.0	0.0	0.0	—	0.582	0.010
— [c]	01:13:38.17	-00:27:39.03	k432	—	—	—	—	—	—	—	—	—
2004hq	02:30:18.04	-08:22:25.01	k441	Ia	Ia-norm	81.0	100.0	0.0	0.0	—	0.680	0.010
2004hp[c]	02:09:35.52	-03:46:23.53	k443	—	—	—	—	—	—	—	—	—
2004hr	01:08:48.34	+00:00:49.49	k448	Ia	Ia-norm	100.0	100.0	0.0	0.0	0.409	0.401	0.005
— [c]	02:31:11.80	-07:47:34.13	k467	—	—	—	—	—	—	—	—	—
2004hs	02:09:33.69	-04:13:03.93	k485	Ia	Ia-norm	93.3	100.0	0.0	0.0	—	0.416	0.005
— [c]	02:30:24.32	-07:53:20.95	k490	—	—	—	—	—	—	0.715	—	—
— [c]	01:08:22.01	-00:05:46.65	m001	—	—	—	—	—	—	—	—	—
—	02:05:27.31	-04:42:54.05	m003	II	—[a]	34.2	2.6	0.0	97.4	—	0.219	0.001
— [c]	02:30:27.27	-09:16:10.23	m006	—	—	—	—	—	—	0.057	—	—
—	02:31:46.24	-09:16:25.65	m010	Ib	Ib-norm	100.0	0.0	100.0	0.0	0.216	0.222	0.001
—	02:08:06.23	-04:03:51.16	m011	II	IIP	78.1	0.0	0.0	100.0	0.205	0.211	0.002
—	02:07:12.91	-04:26:40.06	m014	II	IIP	50.0	0.0	0.0	100.0	0.200	0.212	0.003
—	23:30:02.70	-08:33:36.57	m022	Ia	—[a]	—	93.8	1.8	4.4	—	0.240	0.003
—	23:28:39.97	-09:19:50.00	m026	Ia	—[a]	—	97.8	2.2	0.0	0.655	0.653	0.008
—	01:09:15.01	+00:08:14.80	m027	Ia	Ia-norm	72.2	92.6	7.4	0.0	0.289	0.286	0.006

Table 3—Continued

IAUC ID	RA [J2000]	Dec [J2000]	ESSENCE ID	Type	Subtype	%Subtype	%Ia	%Ib/c	%II	$z_{\rm GAL}$	$z_{\rm SNID}$	σ_z
—	23:29:35.34	-09:58:46.33	m032	Ia	Ia-norm	80.2	96.5	3.5	0.0	—	0.155	0.004
—	02:27:50.33	-07:59:11.62	m034	Ia	Ia-norm	96.3	100.0	0.0	0.0	0.557	0.562	0.006
—	02:05:10.83	-04:47:13.94	m038	II	IIP	94.4	5.6	0.0	94.4	0.051	0.054	0.003
—	02:28:04.63	-07:42:44.29	m039	Ia	Ia-norm	84.4	100.0	0.0	0.0	0.248	0.249	0.003
—	02:09:49.78	-04:45:10.65	m041	II	—[a]	—	22.8	0.0	77.2	—	0.220	0.004
—	23:29:51.73	-08:56:46.07	m043	Ia	Ia-norm	57.3	99.5	0.0	0.5	0.266	0.266	0.003
—	02:10:56.77	-04:27:29.90	m057	Ia	—[a]	—	95.5	0.4	4.1	0.180	0.184	0.003
—	01:09:52.90	+00:36:19.03	m062	Ia	—[a]	—	100.0	0.0	0.0	0.314	0.317	0.005
—	23:24:42.28	-08:29:07.82	m075	Ia	—[a]	—	100.0	0.0	0.0	0.100	0.102	0.001
—	01:08:56.35	+00:39:25.38	m138	Ia	Ia-norm	66.7	100.0	0.0	0.0	0.587	0.582	0.004
—	23:23:57.83	-08:27:08.33	m139	II	—[a]	—	0.0	0.0	100.0	0.212	—	—
—	23:24:03.53	-09:23:18.24	m158	Ia	—[a]	—	95.2	4.8	0.0	—	0.463	0.007
—	02:28:52.20	-07:42:09.78	m193	Ia	Ia-norm	100.0	100.0	0.0	0.0	0.330	0.341	0.009
—	02:06:03.69	-04:39:59.12	m226	Ia	—[a]	—	95.2	4.8	0.0	0.675	0.671	0.004
—[c]	01:14:33.08	-00:26:23.18	n246	—	—	—	—	—	—	0.706	—	—
—	02:28:09.01	-07:47:49.56	n256	Ia	Ia-norm	100.0	100.0	0.0	0.0	—	0.631	0.012
—	02:06:42.35	-04:22:37.01	n258	Ia	Ia-norm	50.0	81.6	18.4	0.0	—	0.522	0.007
—	02:05:14.95	-04:56:39.08	n263	Ia	Ia-norm	79.9	100.0	0.0	0.0	—	0.368	0.007
—	01:13:06.51	+00:30:04.86	n271	II	IIP	85.2	0.0	0.0	100.0	—	0.241	0.004
—	23:28:17.55	-09:23:12.38	n278	Ia	Ia-norm	78.5	100.0	0.0	0.0	0.304	0.309	0.006
—	23:23:51.35	-08:23:18.47	n285	Ia	Ia-norm	64.5	81.4	14.5	4.1	—	0.528	0.006
—[c]	02:29:00.48	-09:02:52.96	n322	—	—	—	—	—	—	—	—	—
—	23:29:58.59	-08:53:12.45	n326	Ia	Ia-norm	79.8	100.0	0.0	0.0	0.264	0.268	0.006
—	23:30:32.01	-10:03:22.14	n368	Ia	Ia-norm	83.1	100.0	0.0	0.0	0.342	0.344	0.006
—[c]	01:13:13.26	-00:23:25.86	n400	—	—	—	—	—	—	0.424	—	—
—	02:31:31.43	-08:55:11.52	n404	Ia	Ia-norm	100.0	100.0	0.0	0.0	—	0.216	0.008
—[c]	02:31:19.60	-08:45:09.76	n406	—	—	—	—	—	—	—	—	—
—	23:29:56.19	-08:34:24.34	p425	Ia	Ia-norm	100.0	100.0	0.0	0.0	0.458	0.453	0.006
—[c]	01:12:40.25	+00:14:56.61	p434	—	—	—	61.7	33.3	4.9	0.339	—	—
—	02:08:32.45	-03:33:34.20	p454	Ia	Ia-norm	100.0	100.0	0.0	0.0	—	0.695	0.010
—	02:11:00.02	-04:09:37.59	p455	Ia	Ia-norm	88.9	100.0	0.0	0.0	0.298	0.284	0.006
—[c]	02:08:09.34	-03:48:05.05	p520	—	—	—	—	—	—	—	—	—
—	02:30:10.16	-08:52:50.84	p524	Ia	Ia-norm	100.0	100.0	0.0	0.0	—	0.508[b]	0.009
—[c]	02:08:10.47	-03:32:17.70	p527	—	—	—	—	—	—	0.435	—	—

4. Photometry of ESSENCE supernovae

4.1. Importance of Photometric Calibration

Our ability to determine cosmological parameters from the observations of supernovae depends on measuring the fluxes of these objects accurately. Errors in photometric calibration translate into errors in the cosmology in two basic ways. First, we must understand the calibration of our supernovae fluxes to those of the low-redshift sample (Hamuy et al. 1993; Riess et al. 1999b; Jha et al. 2006). Light curve fitting and luminosity estimation methods have been trained using these objects and they also serve the "anchor" for the Hubble diagram in our cosmological measurements of the evolution of the scale factor. Second, accurate passband-to-passband calibration is important for estimating the colors of our supernovae, to provide constraints on extinction due to host galaxy dust. See the discussion in Wood-Vasey et al. (2007) for a discussion of how these calibration issues impact our cosmological measurements.

Photometric systems are defined by the broadband fluxes of a single standard star (conventionally Vega, though more recently the Sloan Digital Sky Survey and others have used the F0 subdwarf $BD+17°4708$), as well as a network of standard stars whose fluxes have been calibrated relative to the primary standard (Landolt 1983, 1992), and the wavelength-dependent sensitivities of that system. Observers usually account for the difference between the particular system they are using and the standard system by correcting their observations through terms proportional to the broad-band colors. These linear corrections can be quite accurate when derived from observations of standard stars and then applied to correct the photometry of other stars observed, since stellar spectra are generally relatively smooth. However, supernovae have complex spectra with broad and deep features, and they evolve in time, so the corrections derived from observations of stars are not appropriate for calibrating supernova fluxes into a standard system.

To avoid additional error from converting the observed supernova fluxes to a "standard" system, we report our photometry in the natural system of the CTIO 4m MOSAIC camera:

$$m = -2.5 \log \mathcal{F}(ADU) + zeropoint, \tag{5}$$

where the zeropoints are defined relative to the star Vega. It is important to note that in the process of defining a Vega-based standard star system, the "true" magnitudes of Vega have actually drifted and are slightly non-zero (Bessell et al. 1998; Bohlin & Gilliland 2004; Bohlin 2006). While these offsets amount to changes in the flux scale of only a few percent, they become significant for cosmological measurements at the level of precision we desire

Table 3—Continued

IAUC ID	RA [J2000]	Dec [J2000]	ESSENCE ID	Type	Subtype	%Subtype	%Ia	%Ib/c	%II	$z_{\rm GAL}$	$z_{\rm SNID}$	σ_z
—	02:07:04.66	-03:28:04.37	p528	Ia	Ia-norm	88.2	100.0	0.0	0.0	0.781	0.777	0.005
—	02:04:56.09	-03:49:03.67	p534	Ia	Ia-norm	79.1	100.0	0.0	0.0	0.619	0.615	0.008

[a]A secure type was determined, but not a secure subtype: there was a majority of correlations with one subtype, but the best-match template was of a different subtype.

[b]Only one template which exceeds the cutoff for "good" correlations: the reported redshift is that of the best-match template (as opposed to the median redshift) and the associated error is the formal redshift error for that template (see Blondin & Tonry 2007).

[c]No "good" correlations for this object. No type or redshift information is reported.

[d]While there were "good" correlations for this object, a secure type could not be determined, and we report no redshift for this object.

Note. — **Column Headings:** (1) Official IAU supernova designation; note that not all objects listed here have official International Astronomical Union names; (2) ESSENCE internal identification; (3) Supernova type as determined using SNID (see text for details); (4) Supernova subtype as determined using SNID (see text for details); (5) Absolute fraction of supernova templates corresponding to the supernova subtype listed in column (4); (6) Absolute fraction of supernova templates corresponding to type Ia supernovae; (7) Absolute fraction of supernova templates corresponding to type Ib or Ic supernovae; (8) Absolute fraction of supernova templates corresponding to type II supernovae; (9) Redshift measured from narrow emission or absorption lines from the host galaxy; (10) Redshift as determined using SNID (see text for details); (11) Redshift error on the SNID redshift (see text for details).
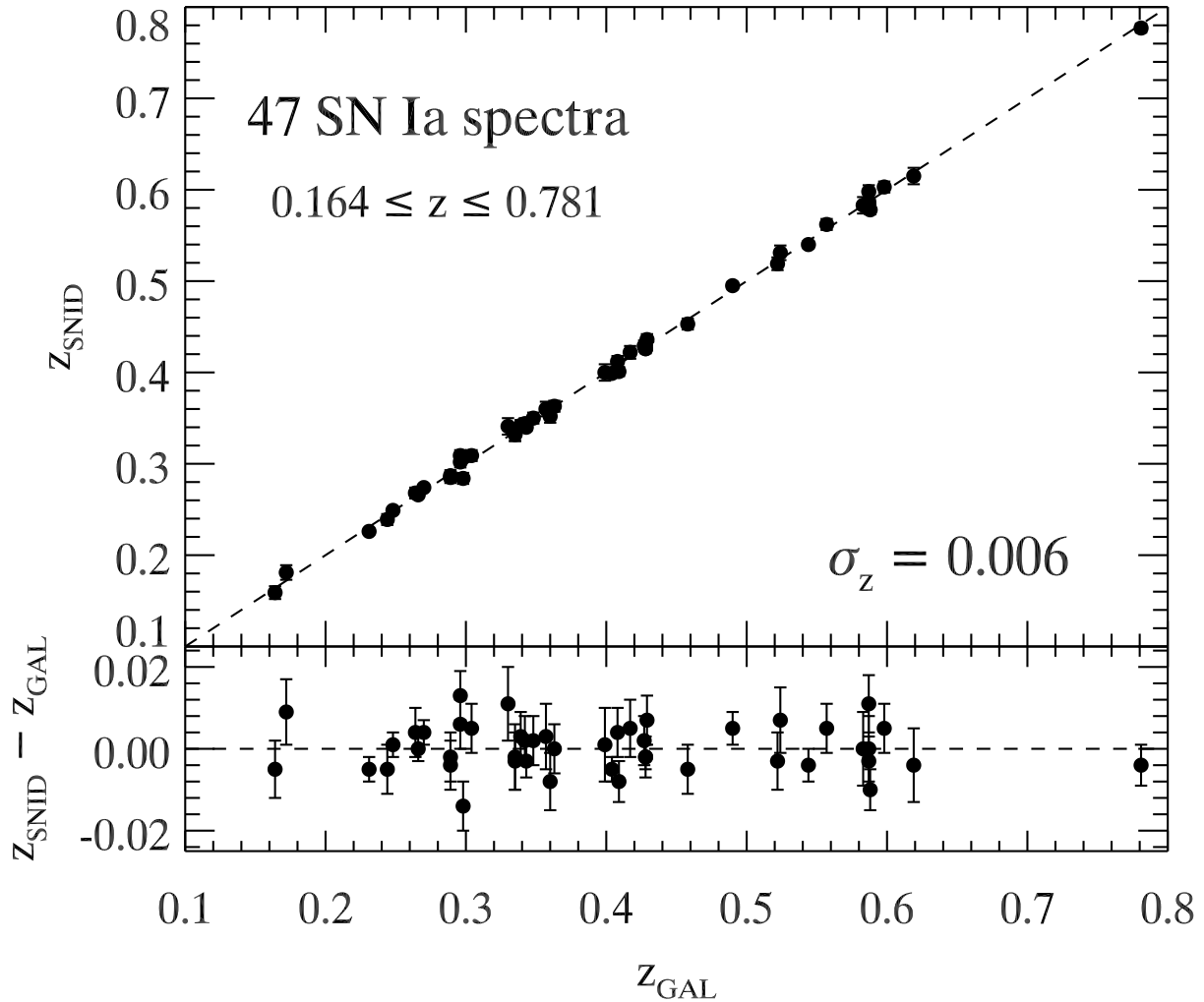
Fig. 4.— Comparison of ESSENCE SN Ia redshifts obtained from narrow emission and/or absorption lines in the host galaxy spectrum (z_{GAL}), and from cross-correlations with a library of SN Ia spectral templates (z_{SN}). The correspondence is excellent, with a standard deviation from the one-to-one correspondence of only ~ 0.006 (see also Matheson et al. 2005). Only the 47 ESSENCE supernovae for which it was possible to measure host galaxy redshifts are used.
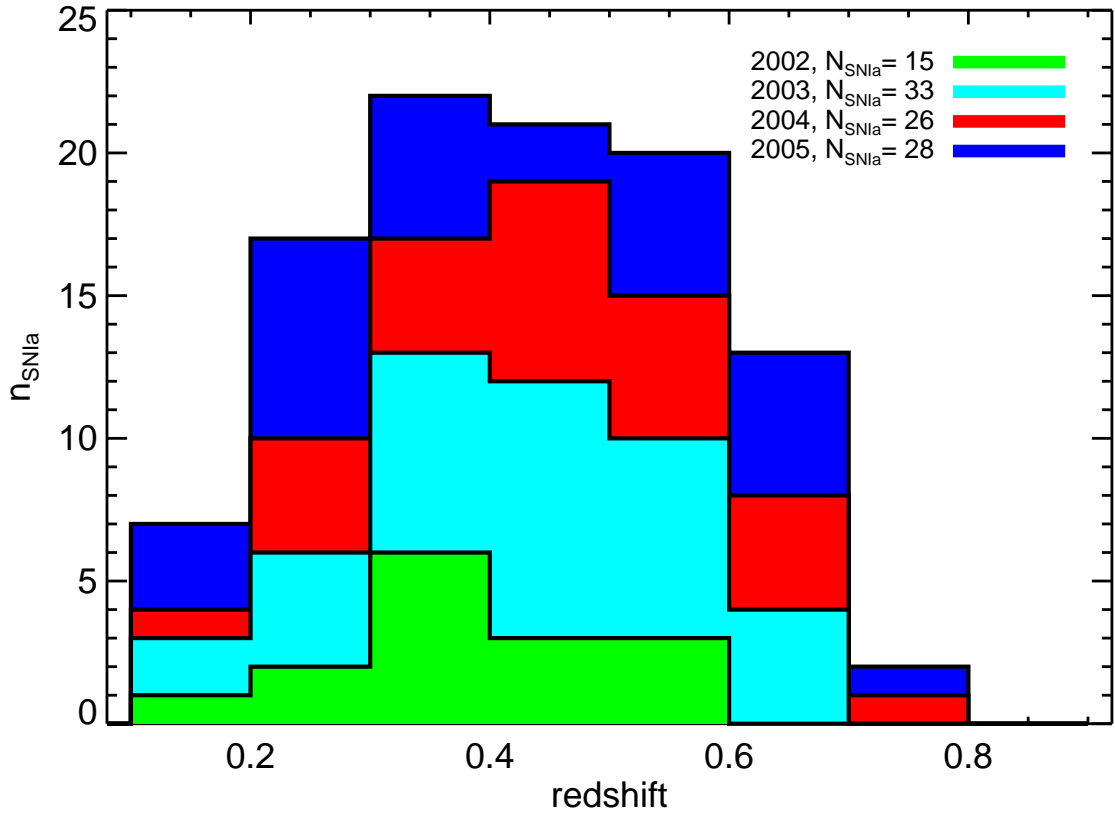
Fig. 5.— Redshift histogram of spectroscopically confirmed ESSENCE SN Ia (all objects whose type Ia correlations exceed 50%).

and must be accounted for (see Wood-Vasey et al. (2007) for our treatment of these in the cosmological analysis).

In the following sections, we describe the calibration of the ESSENCE photometry in the CTIO 4m natural system.

4.2. Calibration of ESSENCE field stars

To establish a Vega-based natural system in our ESSENCE fields, we tie the stars in these fields to the secondary standards of Landolt (1983, 1992). Unfortunately, the overhead in acquiring a sufficient number of observations of these stars with the MOSAIC imager is quite high (∼100 seconds readout time, with additional time spent changing filters and pointing the telescope) relative to the very short exposures needed to observe these bright objects on a 4m class telescope. Therefore we have elected to calibrate stars in our fields with an auxiliary program using the CTIO 0.9m telescope. Concurrent with the ESSENCE program, we have used 16 photometric nights on the 0.9m to observe both Landolt standards and ESSENCE field stars, resulting in 32 calibration patches within the ESSENCE survey. Each patch contains 40-60 stars observed on a minimum of 3 photometric nights. The quality of the photometric calibrations resulting from the 0.9m program is quite good, with individual stars calibrated to ∼1% (Figure 6).

4.3. CTIO 4m photometric zeropoints

While the 0.9m photometry allows for the transfer of photometric calibrations in the Vega system to our 4m data, it is not sufficient to calibrate all of our ESSENCE data, due to the small (13′) field of view relative to the MOSAIC imager. Each 0.9m patch allows us to calibrate data from only one of the 8 CCDs in the CTIO MOSAIC. Therefore, by using our own data taken on photometric nights and carefully propagating photometric zeropoints from the overlapping data to rest of the MOSAIC, we generate catalogs which cover our fields completely. These catalogs effectively define the ESSENCE photometric system and are used to calibrate data taken on all other nights.

First, we must transform the 0.9m magnitudes from the system defined by the Landolt standard stars to the CTIO MOSAIC natural photometric system, via equations of the form:

$$R_{CTIO} = R_{Landolt} + k_{RI}^{R}(R_{Landolt} - I_{Landolt}) \tag{6}$$
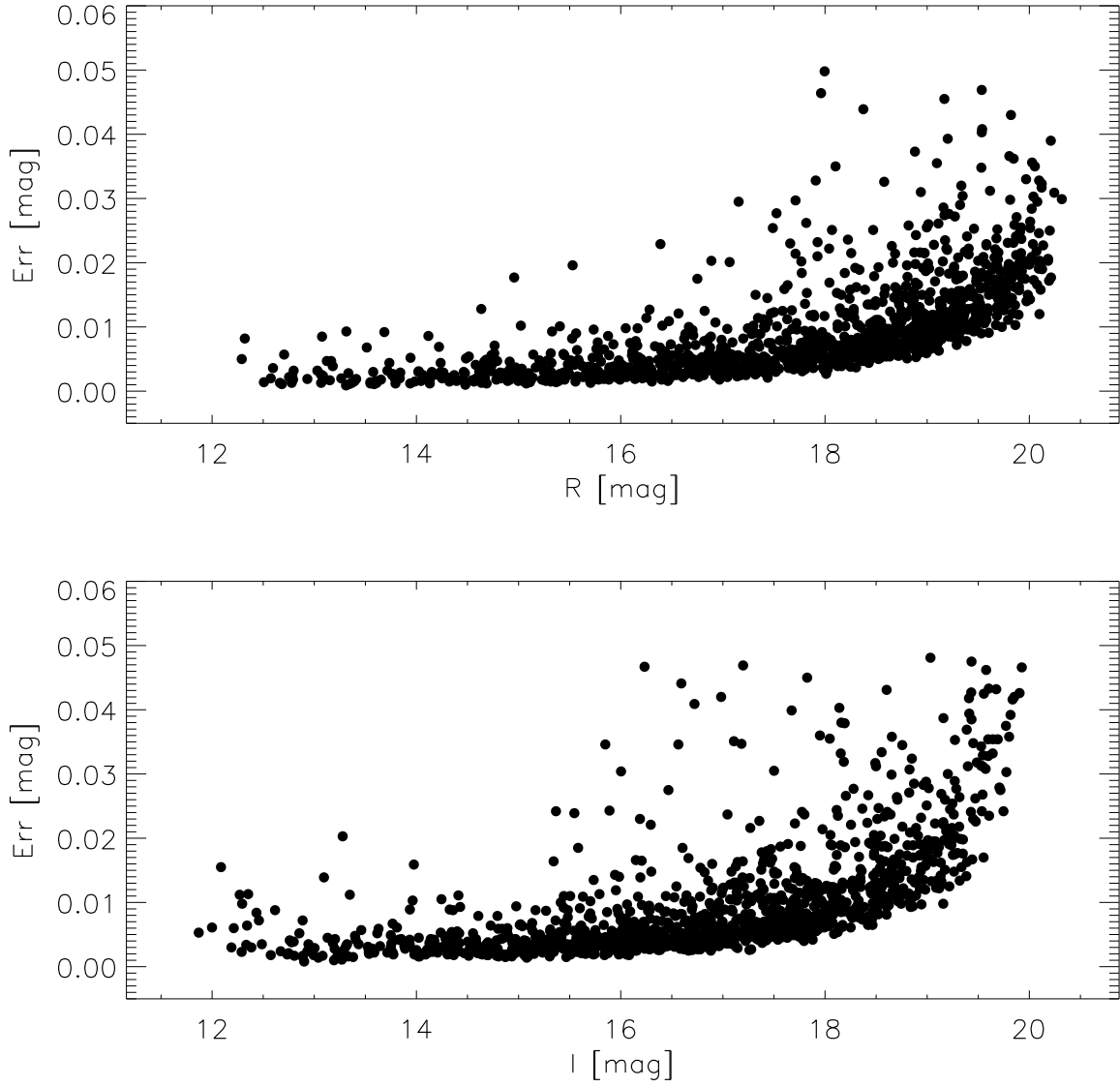
Fig. 6.— Error in 0.9m photometry of ESSENCE field stars as a function of R magnitudes (top panel) and I magnitude (bottom panel). Individual stars are typically measured to a precision of 2% or better.

and

$$I_{CTIO} = I_{Landolt} + k_{RI}^I(R_{Landolt} - I_{Landolt}). \tag{7}$$

Thus we choose to adopt the same zeropoint for R_{CTIO}, I_{CTIO} for stars of zero color in the Landolt system. The color terms k_{RI}^R, k_{RI}^I may then be measured by comparing Landolt standard magnitudes with MOSAIC instrumental magnitudes.

We obtain the values $k_{RI}^R = -0.030$ and $k_{RI}^I = 0.030$ by combining our own work with the information reported on the CTIO 4m web page [4] and with synthetic photometry using 4m MOSAIC passbands and the Stritzinger et al. 2005 spectrophotometric standards. These were also cross-checked by combining aperture corrected DoPHOT magnitudes and 0.9m catalogs.

This 0.9m photometry, now transformed to the CTIO MOSAIC natural photometric system, was used to compute the zero points of the two subfields covered by the 0.9m field of view for each of the ESSENCE fields. To generate catalogs for the other subfields, we must propagate the photometric zeropoint from these subfields across the rest of the MOSAIC. This requires that the instrumental sensitivities are normalized to a common level, such that one data unit corresponds to the same amount of incident flux for every subfield, and that we measure the *same* fraction of the flux for the stars in all the images, which can be achieved by correcting the PSF magnitudes to an aperture which encloses the total flux. If these two conditions are met, then the zeropoint derived for one subfield is valid for the entire MOSAIC.

To ensure that the sensitivities are normalized from subfield to subfield, we use the ratios of the sky levels between subfields, for all the images for a given night to establish these relative flux scalings. Because of the enormous numbers of pixels used to measure this ratio, the results are incredibly precise and the normalization factors can be measured to $\sim 0.3\%$. This method actually normalizes the CCD sensitivities for the spectral energy distribution of the sky, which obviously differs from those of astronomical objects we seek to measure. However, tests using a range of passband sensitivity curves and a variety of input spectra show that the resulting photometric errors are much less than 1%. Though the method is unaffected by uniform variations in sky brightness across the entire MOSAIC, care must be taken to avoid applying this method in the presence of moonlight which could result in a systematic gradient in sky brightness across the array.

---

[4] *http://www.ctio.noao.edu/mosaic/ZeroPoints.html*

We then turn to the photometry of stars in the ESSENCE fields, which have been measured using DoPHOT PSF photometry. To correct these magnitudes so that they measure the total flux for the objects in the images, we use the standard method from aperture photometry of constructing a "growth curve" for each image from the incremental flux in concentric annuli about the objects. We choose a small aperture, for which we robustly determine the offset between the PSF magnitudes and aperture magnitudes for the brightest stars in the image. We then construct a growth curve out to an aperture at large enough radius that the flux measured at those annuli is consistent with zero. Such aperture corrections are calculated for each subfield-image in a field and are then used to bring all of the PSF photometry onto the same flux scale. Note that while the PSF does vary across the field of view of the MOSAIC, the small number of isolated stars in a typical ESSENCE field makes robust determination of spatially varying aperture corrections difficult, so instead a single correction is calculated for each subfield-image.

With the photometry of the stars in all subfields now on the same flux scaling, we are able to propagate photometric zero points across the whole MOSAIC. In this manner, we calibrate magnitudes for all the stars present in our fields for several epochs and then compute σ-clipped averages over all of the measurements. Figure 7 demonstrates there is a small dispersion in the residuals about the mean for all the stars in our catalogs. This shows that the zeropoint propagation procedure is robust from night to night.

To check the field to field consistency of these catalogs, we consider the ESSENCE data taken under photometric conditions. For a given night, we correct the zero points for each by applying aperture and airmass correction. We then take the average value of those corrected zero points as the true zeropoint for the entire night. We then also calibrate each field individually, using our photometric catalogs. In Figure 8, we show the distribution of the differences between the zeropoints calculated using the ESSENCE catalogs and the average nightly zeropoint. The small scatter of 0.02 magnitudes in each passband assures us that the zeropoints are consistent from field to field with a precision of better than 2%.
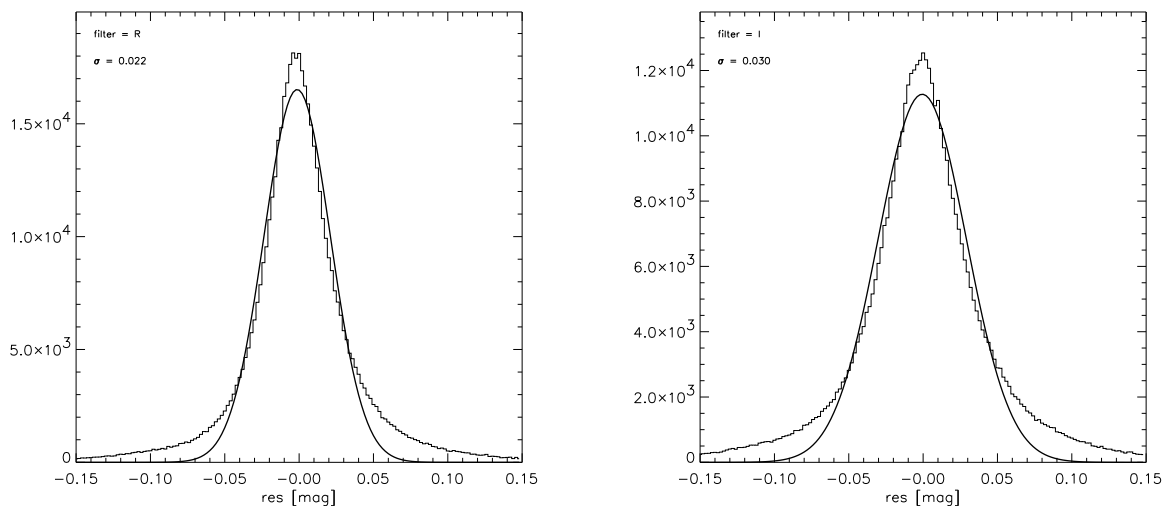
Fig. 7.— Distribution of the night-to-night photometric residuals in magnitudes for CTIO 4m R (left plot) and I band (right plot) bands for ESSENCE field stars. The solid lines are Gaussians fit to the data. The small widths of the histograms ($\sim$2-3%) demonstrates the temporal stability of our photometry.
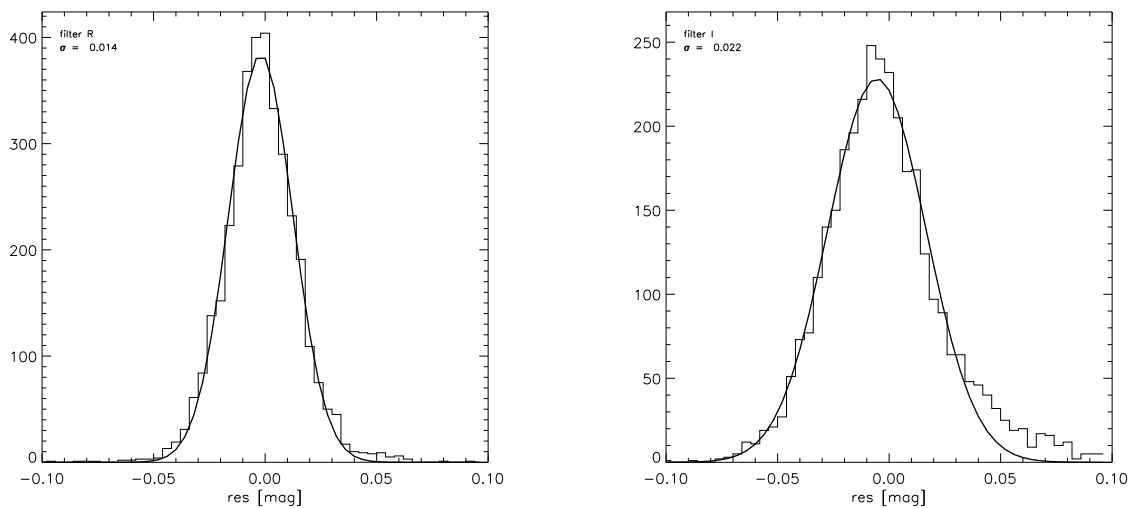
Fig. 8.— Distribution of photometric zeropoint residuals, in magnitudes, for the R (left plot) and I band (right plot) bands. The small scatter of $\sim$1-2% demonstrates that our zeropoints are homogenous across the ESSENCE fields. The solid lines are Gaussians fit to the data.

4.4. Supernova flux measurement

With accurately determined fluxes of the stars in our fields in the natural system, we then seek to measure the supernova fluxes as accurately as possible. This requires that we remove the background light due to the host galaxy, via image subtraction using the same software as in the search pipline (section 2.2.5). It is crucial that the subtraction procedure maintains the flux scaling from the original image, which has been calibrated to stars, through to the subtracted image, where we measure the supernova flux. We have performed extensive tests by adding synthetic stars to our data to verify that the registration and subtraction processes do not bias the supernova photometry.

To test whether the image registration and subtraction stages affect our photometry, we added thousands of synthetic stars in a subsample of our images before these steps. The flux of those stars was then measured after image registration and after template subtraction respectively. The results are shown in Figures 9 and 10. We find that image registration and subtraction do not significantly bias our photometry, though the nominal photometric error from our noise maps slightly underestimates the true photometric error.

To further study the errors in our photometry as estimated using the noise maps, we measure fluxes using the DoPHOT PSF in a regular grid across the difference image, where there are no sources of flux. If the nominal photometric error were accurate, then we should find that the distribution of flux/σ_{flux} measured with the PSF in these empty regions should be centered on zero with a σ of 1.0. In practice, we find that this distribution is somewhat broader ($\sigma \sim 1.2$) for a typical difference image. We interpret this to mean our errors are slightly underestimated, probably due to pixel-to-pixel covariances generated in the remapping and convolution steps that are not accounted for properly in the noise maps. We scale up the photometric errors for each difference image by the factor 1.2.

On each difference frame, the PSF used to measure the supernova is determined using field stars prior to subtraction. For each subtraction, we convolve the image with the narrower PSF to match the broader PSF in the other image, it is this broader PSF which is used to measure the supernova in the subtraction. The flux calibration of that same image, from comparing DoPHOT photometry to the catalogs described in Section 4.1, is scaled by the normalization of the subtraction kernel and then then applied to the supernova flux measured in the difference image.

To measure the supernova flux accurately, we fix the PSF to the best measured location of the supernova, rather than allow the position to be a free parameter in the PSF fit. Because fitting the PSF at a position displaced from the true source center would result in a systematic underestimate of the measured flux for the entire light curve, we estimate the size
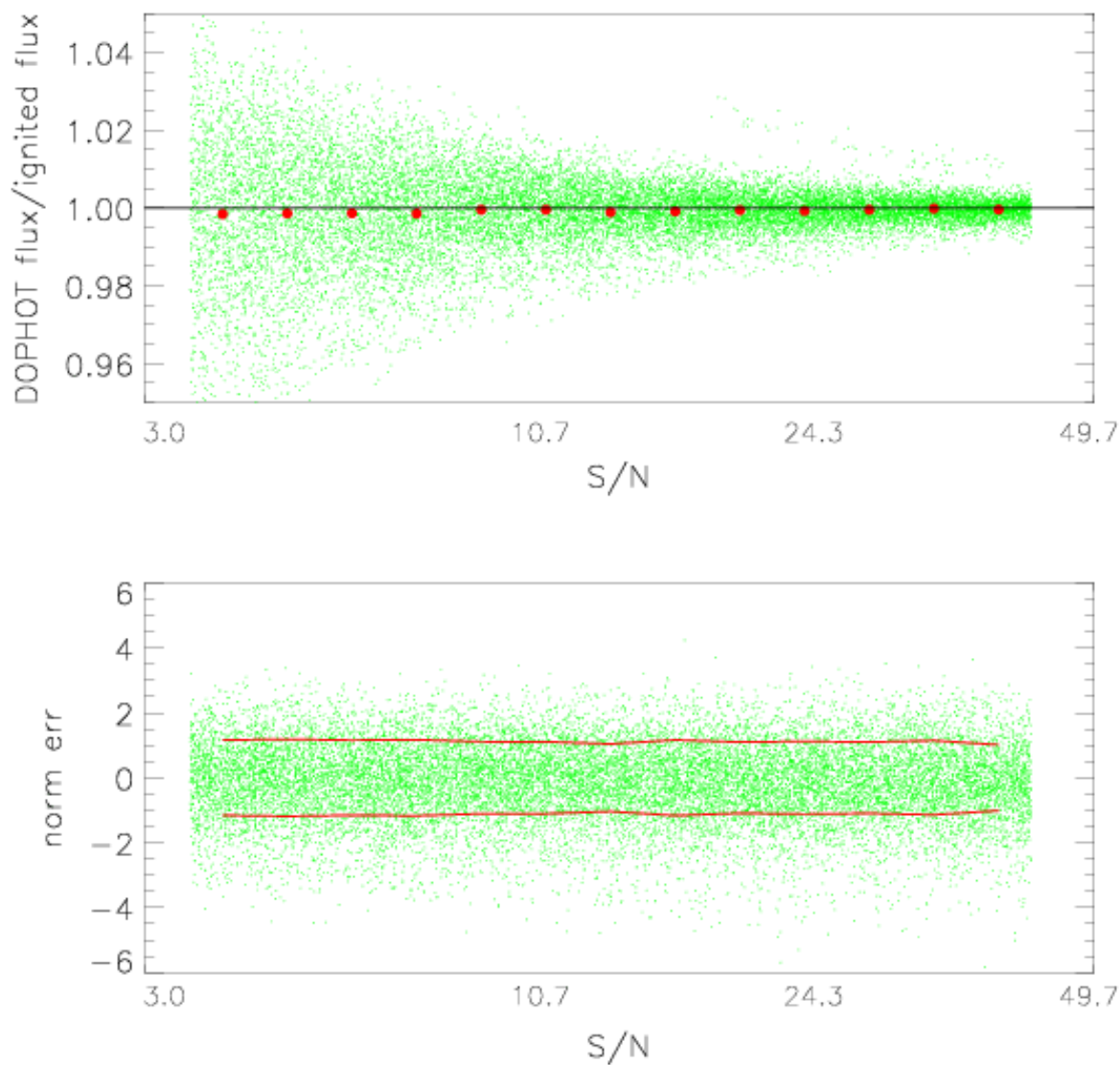
Fig. 9.— Fake stars were added to images before remapping, which rebins pixels. The top panel shows the ratio of the flux measured to the input flux in the rebinned image, as a function of the signal-to-noise ratio of the fake star. Green points are individual stars, red points are averages. Rebinning does not significantly bias our photometry, even at low SNR. The bottom panel shows the ratio of the flux residuals (input flux - measured flux) divided by the estimated error using our noise maps, as a function of SNR. The red lines denote one standard deviation. We find that the distribution is slightly broader than expected ($\sigma = 1.1$), indicating that our nominal error computed using the noise maps slightly underestimates the actual error by 10%.
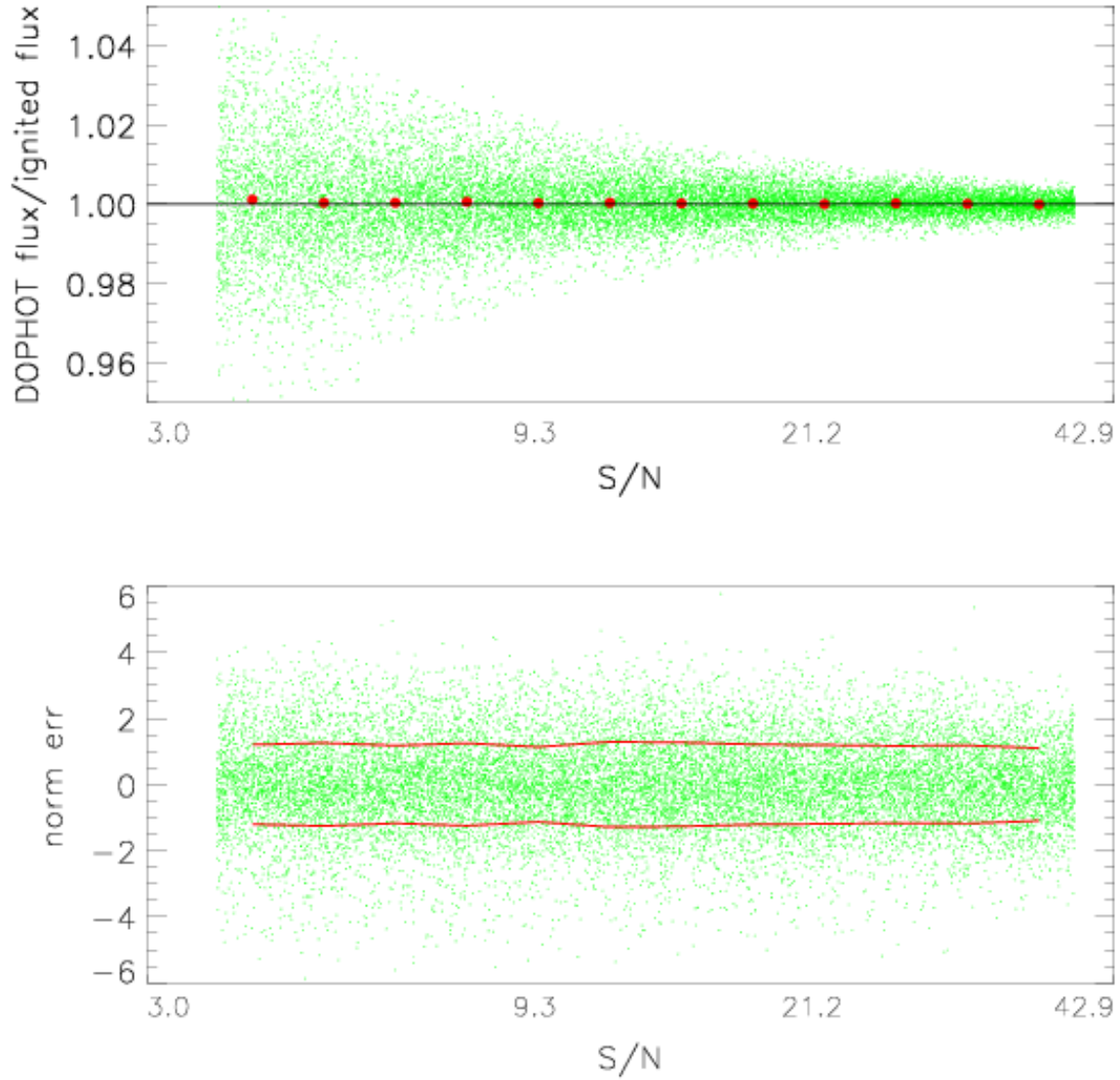
Fig. 10.— Same as Figure 9, except the fake stars have been remeasured after template subtraction. The photometry remains linear to much better than 1%, even at low SNR. The normalized error distribution has $\sigma = 1.2$, so we scale the photometric error of measurements on subtracted images up by 20% from the value obtained from the noise maps.

of this effect for our typical positional errors. The location for each supernova is refined from its discovery position by taking the average of all detections with a signal-to-noise ratio of 5 or greater in all the available difference image frames . These derived positions are accurate to within $0.02''$ within our astrometric system. In Fig. 11 such a systematic is quantified by artificially shifting sources of known flux that have a FWHM of 1.0 arcsec, the average value for the ESSENCE survey. Our SN light curves are usually very well sampled, providing a cumulative signal-to-noise ratio greater than 10 even for the highest redshift objects. This effective signal-to-noise ratio translates to a photometric error less than 1.0%.

To obtain optimal signal-to-noise in our subtractions, we make use of all of the images that contain background galaxy light. We follow the methodology outlined in Barris et al. (2005), which utilizes the flux differences from all $N(N-1)/2$ possible image pairs to estimate the supernova flux.

When dealing with the thousands of difference images generated in our NN2 method, automated and quantitative quality controls were crucial in extracting good measurements. A second check was to measure the flux of known stars in the difference image. Ideally, there should be no excess of positive or negative flux in the remaining if the subtraction process was successful. After sigma-clipping to reject variable stars, the average flux/σ_{flux} at the positions of all the stars was measured and if it was inconsistent with the flux uncertainty expected for the difference image, that difference image was not used to measure the supernova flux. Once the quality-controlled full sets of N*(N-1)/2 data files were generated, they were run through the nn2 program of Barris et al. (2005) to generate our final supernova light curves included in this paper.
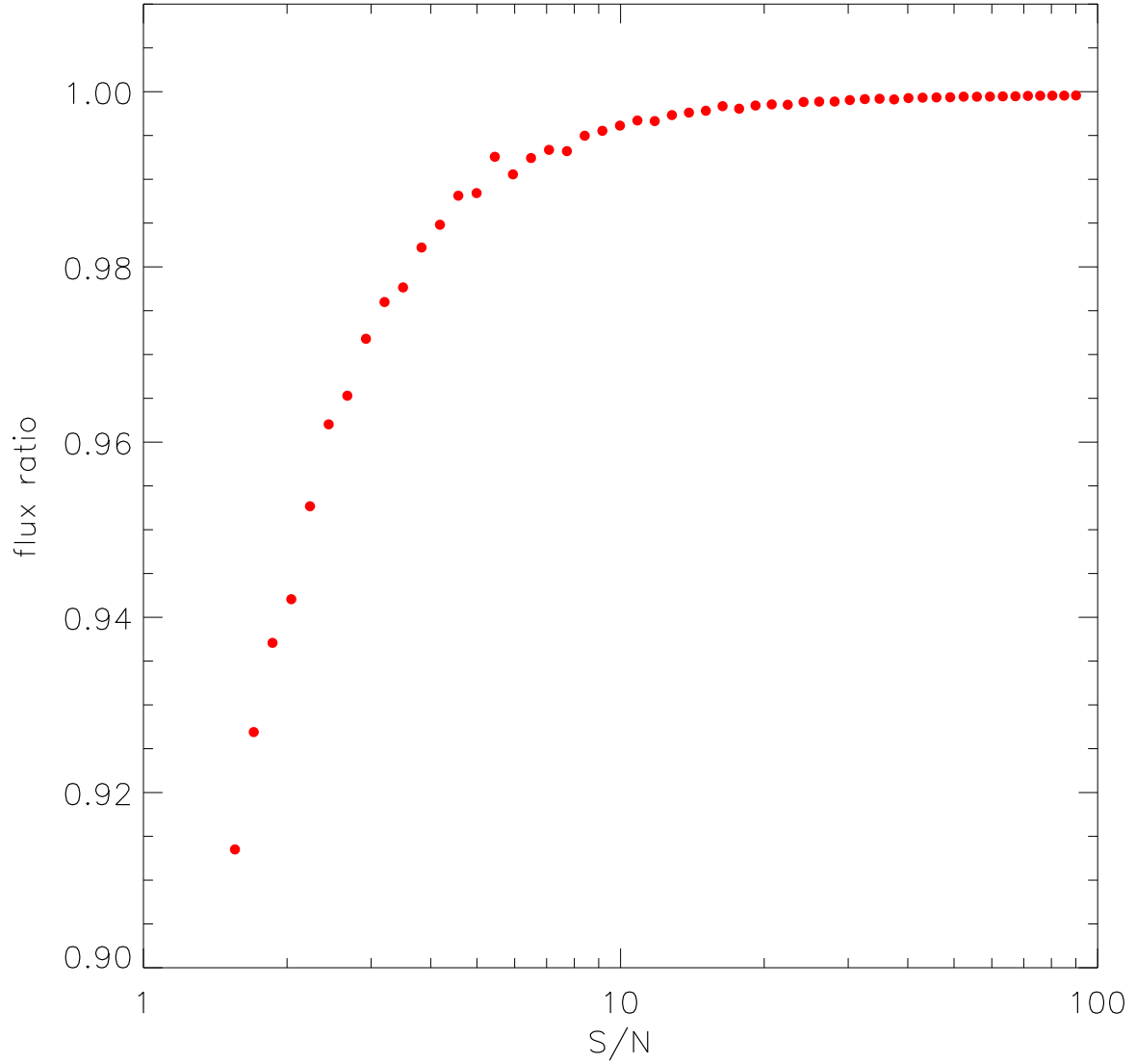
Fig. 11.— Ratio of recovered to input flux due to systematic misalignment of the PSF for the typical centroiding error as a function of the cumulative signal-to-noise ratio of the object over all photometric measurements. By combining all measurements in both passbands, the positions of even faint SNe are constrained at a level corresponding to SNR ¿ 10.

5. Photometry from the ESSENCE four year sample

We present here four sample ESSENCE light curve to illustrate the quality of the ESSENCE photometry (Figure 12). These objects were chosen to be closest in redshift to an abitrary set of redshifts, $z = 0.20, 0.35, 0.50, 0.65$, which span the range of the ESSENCE redshift distribution. For the purposes of plotting, all data from the season in which the SN was discovered are displayed. Photometry is presented in linear flux units in the CTIO 4m natural system, where the formula for conversion to standard magnitudes is

$$m = -2.5 \log \mathcal{F} + 25. \tag{8}$$

Since the photometry is reported in the CTIO 4m natural system, the system throughput curves are an integral part of the data set and are presented here as well (Figure 13). These system throughput curves are the product of:

- the CTIO MOSAIC R and I filters, as measured in the laboratory,

- standard quantum efficiency curves for the CCDs from the, manufacturer (Tek),

- the wavelength dependence of aluminum, for the two surfaces in the 4m telescope and

- typical atmospheric transmissivity, with losses due to scattering and molecular absorption, calculated from taking the observations of spectrophotometric standards (Hamuy et al. 1995) with Bessell's removal of the telluric features (Bessell 1999) to determine the average atmospheric absorption at CTIO.

We are also developing a novel technique for measuring the full wavelength-dependent response of the telescope/camera system through the use of a tunable laser and a calibrated photo-diode Stubbs & Tonry (2006). Preliminary results from this new method are consistent with the estimates we derived from the product of each component as described above.

The full set of ESSENCE light curves and system throughput curves are available electronically at `http://www.ctio.noao.edu/essence/`.
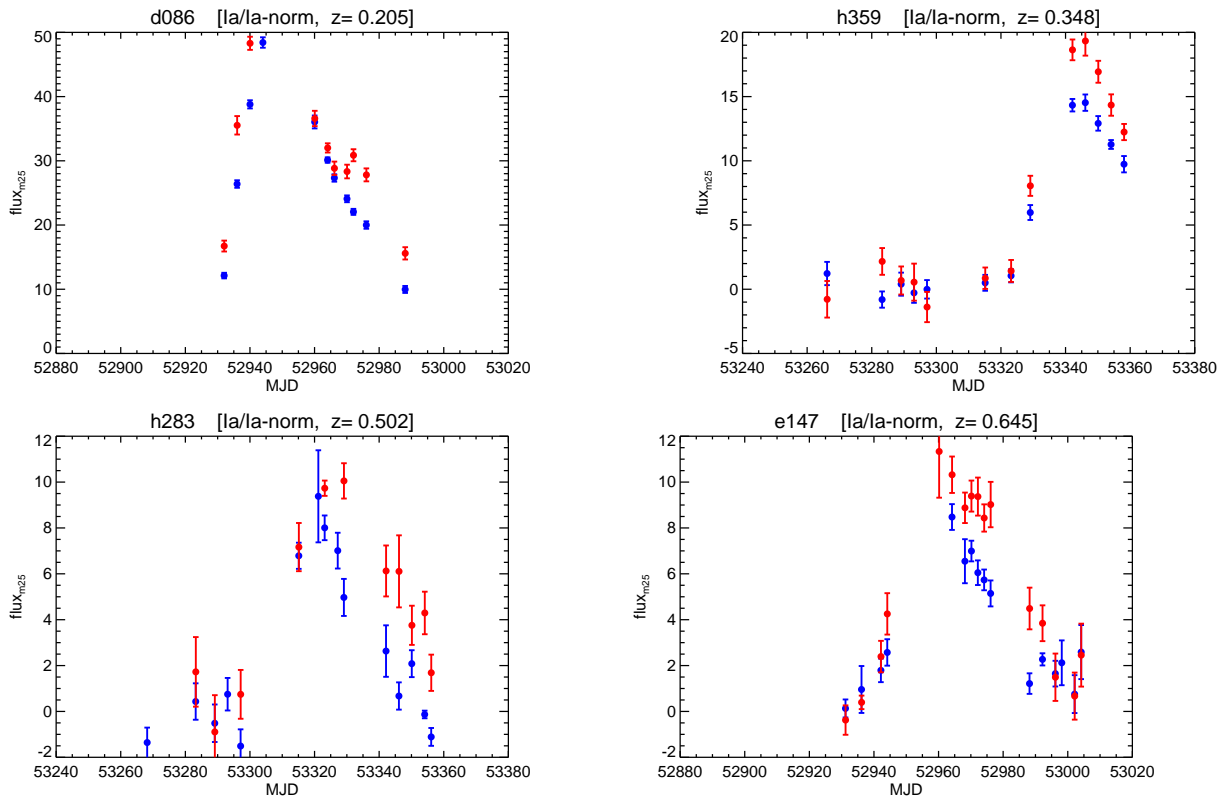
Fig. 12.— Example ESSENCE light curves, in units of linear flux, scaled such that flux=1 corresponds to magnitude 25 (blue=R, red=I). Only data from the observing season in which the object was discovered are plotted.

6. Conclusion

We have presented the scientific motivation for the ESSENCE survey, which aims to constrain the equation of state parameter of dark energy, w, to 10%. Modelling our survey suggests there is a slight gain in the accuracy of measuring w by covering a greater volume at lower redshifts by pushing the survey to relatively short exposure times. We describe how, using the survey strategy and software outlined here, we detect likely high-redshift supernovae using rapid analysis of survey data and how we analyze spectroscopic data to confidently identify objects as type Ia supernovae and measure their redshifts. The photometry for these 102 SN Iais presented here, in the CTIO 4m natural system, as detailed in this document.

Once we have identified the sample of good type Ia supernovae and carefully measured their light curves, the next step is to estimate distances to these objects. A detailed description of the process of turning supernova photometry and redshifts to cosmological distances and finally, constraints on cosmological parameters follows in a companion paper (Wood-Vasey et al. 2007).

ESSENCE has two remaining years of operation. In addition to increasing the sample size, we are undertaking a focused effort to improve the photometric calibration of the CTIO4m and thus reduce the potential systematic errors from miscalibration. This program has been awarded nine nights of engineering time specifically for the goal of improving the MOSAIC calibrations via concentrated observations of standard star fields, along with fields observed by ESSENCE and other on-going CTIO 4m surveys. With a final sample of ~ 150 type Ia SNe and an improvement in photometric precision from the current 2% to a final 1%, we will reach the goal of the project: a measurement of w to 10%.

7. Acknowledgments

REFERENCES

Alard, C. 2000, A&AS, 144, 363

Alard, C. & Lupton, R. H. 1998, ApJ, 503, 325

Albrecht, A., Bernstein, G., Cahn, R., Freedman, W. L., Hewitt, J., Hu, W., Huth, J., Kamionkowski, M., Kolb, E. W., Knox, L., Mather, J. C., Staggs, S., & Suntzeff, N. B. 2006, ArXiv Astrophysics e-prints

Appenzeller, I., Fricke, K., Furtig, W., Gassler, W., Hafner, R., Harkl, R., Hess, H.-J., Hummel, W., Jurgens, P., Kudritzki, R.-P., Mantel, K.-H., Meisl, W., Muschielok, B., Nicklas, H., Rupprecht, G., Seifert, W., Stahl, O., Szeifert, T., & Tarantik, K. 1998, The Messenger, 94, 1

Astier, P., Guy, J., Regnault, N., Pain, R., Aubourg, E., Balam, D., Basa, S., Carlberg, R. G., Fabbro, S., Fouchez, D., Hook, I. M., Howell, D. A., Lafoux, H., Neill, J. D., Palanque-Delabrouille, N., Perrett, K., Pritchet, C. J., Rich, J., Sullivan, M., Taillet, R., Aldering, G., Antilogus, P., Arsenijevic, V., Balland, C., Baumont, S., Bronder, J., Courtois, H., Ellis, R. S., Filiol, M., Gonçalves, A. C., Goobar, A., Guide, D., Hardin, D., Lusset, V., Lidman, C., McMahon, R., Mouchet, M., Mourao, A., Perlmutter, S., Ripoche, P., Tao, C., & Walton, N. 2006, A&A, 447, 31

Barris, B. J., Tonry, J. L., Blondin, S., Challis, P., Chornock, R., Clocchiatti, A., Filippenko, A. V., Garnavich, P., Holland, S. T., Jha, S., Kirshner, R. P., Krisciunas, K., Leibundgut, B., Li, W., Matheson, T., Miknaitis, G., Riess, A. G., Schmidt, B. P., Smith, R. C., Sollerman, J., Spyromilio, J., Stubbs, C. W., Suntzeff, N. B., Aussel, H., Chambers, K. C., Connelley, M. S., Donovan, D., Henry, J. P., Kaiser, N., Liu, M. C., Martín, E. L., & Wainscoat, R. J. 2004, ApJ, 602, 571

Barris, B. J., Tonry, J. L., Novicki, M. C., & Wood-Vasey, W. M. 2005, The NN2 Flux Difference Method for Constructing Variable Object Light Curves

Benetti, S., Cappellaro, E., Turatto, M., Taubenberger, S., Harutyunyan, A., & Valenti, S. 2006, ArXiv Astrophysics e-prints

Bertin, E., Mellier, Y., Radovich, M., Missonnier, G., Didelon, P., & Morin, B. ASP Conf. Ser. 281: Astronomical Data Analysis Software and Systems XI, ed. , D. A. BohlenderD. Durand & T. H. Handley, 228–+

Bessell, M. S. 1999, PASP, 111, 1426

Bessell, M. S., Castelli, F., & Plez, B. 1998, A&A, 333, 231

Blondin, S. & Tonry, J. 2007

Blondin, S., Walsh, J. R., Leibundgut, B., & Sainton, G. 2005, A&A, 431, 757

Bohlin, R. C. 2006, ArXiv Astrophysics e-prints

Bohlin, R. C. & Gilliland, R. L. 2004, AJ, 127, 3508

Branch, D., Livio, M., Yungelson, L. R., Boffi, F. R., & Baron, E. 1995, PASP, 107, 1019

Candia, P., Krisciunas, K., Suntzeff, N. B., González, D., Espinoza, J., Leiton, R., Rest, A., Smith, R. C., Cuadra, J., Tavenner, T., Logan, C., Snider, K., Thomas, M., West, A. A., González, G., González, S., Phillips, M. M., Hastings, N. C., & McMillan, R. 2003, PASP, 115, 277

Carroll, S. M., Press, W. H., & Turner, E. L. 1992, ARA&A, 30, 499

Clocchiatti, A., Schmidt, B. P., Filippenko, A. V., Challis, P., Coil, A. L., Covarrubias, R., Diercks, A., Garnavich, P., Germany, L., Gilliland, R., Hogan, C., Jha, S., Kirshner, R. P., Leibundgut, B., Leonard, D., Li, W., Matheson, T., Phillips, M. M., Prieto, J. L., Reiss, D., Riess, A. G., Schommer, R., Smith, R. C., Soderberg, A., Spyromilio, J., Stubbs, C., Suntzeff, N. B., Tonry, J. L., & Woudt, P. 2006, ApJ, 642, 1

Colgate, S. A. & McKee, C. 1969, ApJ, 157, 623

Conley, A., Howell, D. A., Howes, A., Sullivan, M., Astier, P., Balam, D., Basa, S., Carlberg, R. G., Fouchez, D., Guy, J., Hook, I., Neill, J. D., Pain, R., Perrett, K., Pritchet, C. J., Regnault, N., Rich, J., Taillet, R., Aubourg, E., Bronder, J., Ellis, R. S., Fabbro, S., Filiol, M., Le Borgne, D., Palanque-Delabrouille, N., Perlmutter, S., & Ripoche, P. 2006, AJ, 132, 1707

Contardo, G., Leibundgut, B., & Vacca, W. D. 2000, A&A, 359, 876

Dressler, A. 2004, A User's Manual for IMACS [LINK]

Dvali, G., Gabadadze, G., & Shifman, M. 2003, Phys. Rev. D, 67, 044020

Eisenstein, D. J., Zehavi, I., Hogg, D. W., Scoccimarro, R., Blanton, M. R., Nichol, R. C., Scranton, R., Seo, H.-J., Tegmark, M., Zheng, Z., Anderson, S. F., Annis, J., Bahcall, N., Brinkmann, J., Burles, S., Castander, F. J., Connolly, A., Csabai, I., Doi, M., Fukugita, M., Frieman, J. A., Glazebrook, K., Gunn, J. E., Hendry, J. S., Hennessy, G., Ivezić, Z., Kent, S., Knapp, G. R., Lin, H., Loh, Y.-S., Lupton, R. H., Margon, B., McKay, T. A., Meiksin, A., Munn, J. A., Pope, A., Richmond, M. W., Schlegel, D., Schneider, D. P., Shimasaku, K., Stoughton, C., Strauss, M. A., SubbaRao, M., Szalay, A. S., Szapudi, I., Tucker, D. L., Yanny, B., & York, D. G. 2005, ApJ, 633, 560

Faber, S. M., Phillips, A. C., Kibrick, R. I., Alcott, B., Allen, S. L., Burrous, J., Cantrall, T., Clarke, D., Coil, A. L., Cowley, D. J., Davis, M., Deich, W. T. S., Dietsch, K., Gilmore, D. K., Harper, C. A., Hilyard, D. F., Lewis, J. P., McVeigh, M., Newman, J., Osborne, J., Schiavon, R., Stover, R. J., Tucker, D., Wallace, V., Wei, M., Wirth, G., & Wright, C. A. 2003, in Instrument Design and Performance for Optical/Infrared Ground-based Telescopes. Edited by Iye, Masanori; Moorwood, Alan F. M. Proceedings of the SPIE, Volume 4841, pp. 1657-1669 (2003)., ed. M. e. a. Iye, 1657–1669

Fabricant, D., Cheimets, P., Caldwell, N., & Geary, J. 1998, PASP, 110, 79

Filippenko, A. V. 1997, ARA&A, 35, 309

Freedman, W. L. & Turner, M. S. 2003, Reviews of Modern Physics, 75, 1433

Frieman, J., Adelman-McCarthy, J., Barentine, J., Becker, A., Boroski, W., Brewington, H., Connolly, A., DeJongh, F., Dembicky, J., Dilday, B., Doi, M., Gunn, J., Harvanek, M., Hawley, S., Hoeflich, P., Hogan, C., Holtzman, J., Johnston, D., Kaplan, J., Kessler, R., Ketzeback, B., Kilper, G., Kleinman, A., Kleinman, S., Kron, R. G., Krughoff, S., Krzesinski, J., Lamenti, D., Lampeitl, H., Long, D., Marriner, J., McMillan, R., Miknaitis, G., Newman, P. R., Nichol, R., Riess, A., Romani, R., Sako, M., Scranton, R., Snedden, S., Stoughton, C., Subbarao, M., Tucker, D., Wang, L., Yasuda, N., York, D., & SDSS. 2004, in Bulletin of the American Astronomical Society, 1548–+

Gallagher, J. S., Garnavich, P. M., Berlind, P., Challis, P., Jha, S., & Kirshner, R. P. 2005, ApJ, 634, 210

Garg, A., Stubbs, C. W., Challis, P., Wood-Vasey, W. M., Blondin, S., Huber, M. E., Cook, K., Nikolaev, S., Rest, A., Smith, R. C., Olsen, K., Suntzeff, N. B., Aguilera, C., Prieto, J. L., Becker, A., Miceli, A., Miknaitis, G., Clocchiatti, A., Minniti, D., Morelli, L., & Welch, D. L. 2006, ArXiv Astrophysics e-prints

Garnavich, P. M., Jha, S., Challis, P., Clocchiatti, A., Diercks, A., Filippenko, A. V., Gilliland, R. L., Hogan, C. J., Kirshner, R. P., Leibundgut, B., Phillips, M. M., Reiss, D., Riess, A. G., Schmidt, B. P., Schommer, R. A., Smith, R. C., Spyromilio, J., Stubbs, C., Suntzeff, N. B., Tonry, J., & Carroll, S. M. 1998, ApJ, 509, 74

Goldhaber, G., Groom, D. E., Kim, A., Aldering, G., Astier, P., Conley, A., Deustua, S. E., Ellis, R., Fabbro, S., Fruchter, A. S., Goobar, A., Hook, I., Irwin, M., Kim, M., Knop, R. A., Lidman, C., McMahon, R., Nugent, P. E., Pain, R., Panagia, N., Pennypacker, C. R., Perlmutter, S., Ruiz-Lapuente, P., Schaefer, B., Walton, N. A., & York, T. 2001, ApJ, 558, 359

Guy, J., Astier, P., Nobili, S., Regnault, N., & Pain, R. 2005, A&A, 443, 781

Hamuy, M., Maza, J., Phillips, M. M., Suntzeff, N. B., Wischnjewsky, M., Smith, R. C., Antezana, R., Wells, L. A., Gonzalez, L. E., Gigoux, P., Navarrete, M., Barrientos, F., Lamontagne, R., della Valle, M., Elias, J. E., Phillips, A. C., Odewahn, S. C., Baldwin, J. A., Walker, A. R., Williams, T., Sturch, C. R., Baganoff, F. K., Chaboyer, B. C., Schommer, R. A., Tirado, H., Hernandez, M., Ugarte, P., Guhathakurta, P., Howell, S. B., Szkody, P., Schmidtke, P. C., & Roth, J. 1993, AJ, 106, 2392

Hamuy, M., Phillips, M. M., Suntzeff, N. B., Maza, J., González, L. E., Roth, M., Krisciunas, K., Morrell, N., Green, E. M., Persson, S. E., & McCarthy, P. J. 2003, Nature, 424, 651

Hamuy, M., Phillips, M. M., Suntzeff, N. B., Schommer, R. A., Maza, J., & Aviles, R. 1996, AJ, 112, 2398

Hamuy, M., Trager, S. C., Pinto, P. A., Phillips, M. M., Schommer, R. A., Ivanov, V., & Suntzeff, N. B. 2000, AJ, 120, 1479

Hamuy, M., Walker, A. R., Suntzeff, N. B., Gigoux, P., Heathcote, S. R., & Phillips, M. M. 1995, VizieR Online Data Catalog, 2179, 0

Hatano, K., Branch, D., & Deaton, J. 1998, ApJ, 502, 177

Hillebrandt, W. & Niemeyer, J. C. 2000, ARA&A, 38, 191

Hook, I., Allington-Smith, J. R., Beard, S. M., Crampton, D., Davies, R. L., Dickson, C. G., Ebbers, A. W., Fletcher, J. M., Jorgensen, I., Jean, I., Juneau, S., Murowinski, R. G., Nolan, R., Laidlaw, K., Leckie, B., Marshall, G. E., Purkins, T., Richardson, I. M., Roberts, S. C., Simons, D. A., Smith, M. J., Stilburn, J. R., Szeto, K., Tierney, C., Wolff, R. J., & Wooff, R. 2003, in Instrument Design and Performance for Optical/Infrared Ground-based Telescopes. Edited by Iye, Masanori; Moorwood, Alan F. M. Proceedings of the SPIE, Volume 4841, pp. 1645-1656 (2003)., 1645–1656

Horne, K. 1986, PASP, 98, 609

Hoyle, F. & Fowler, W. A. 1960, ApJ, 132, 565

Jha, S. 2002, Ph.D. Thesis

Jha, S., Kirshner, R. P., Challis, P., Garnavich, P. M., Matheson, T., Soderberg, A. M., Graves, G. J. M., Hicken, M., Alves, J. F., Arce, H. G., Balog, Z., Barmby, P., Barton, E. J., Berlind, P., Bragg, A. E., Briceño, C., Brown, W. R., Buckley, J. H., Caldwell,

N., Calkins, M. L., Carter, B. J., Concannon, K. D., Donnelly, R. H., Eriksen, K. A., Fabricant, D. G., Falco, E. E., Fiore, F., Garcia, M. R., Gómez, M., Grogin, N. A., Groner, T., Groot, P. J., Haisch, Jr., K. E., Hartmann, L., Hergenrother, C. W., Holman, M. J., Huchra, J. P., Jayawardhana, R., Jerius, D., Kannappan, S. J., Kim, D.-W., Kleyna, J. T., Kochanek, C. S., Koranyi, D. M., Krockenberger, M., Lada, C. J., Luhman, K. L., Luu, J. X., Macri, L. M., Mader, J. A., Mahdavi, A., Marengo, M., Marsden, B. G., McLeod, B. A., McNamara, B. R., Megeath, S. T., Moraru, D., Mossman, A. E., Muench, A. A., Muñoz, J. A., Muzerolle, J., Naranjo, O., Nelson-Patel, K., Pahre, M. A., Patten, B. M., Peters, J., Peters, W., Raymond, J. C., Rines, K., Schild, R. E., Sobczak, G. J., Spahr, T. B., Stauffer, J. R., Stefanik, R. P., Szentgyorgyi, A. H., Tollestrup, E. V., Väisänen, P., Vikhlinin, A., Wang, Z., Willner, S. P., Wolk, S. J., Zajac, J. M., Zhao, P., & Stanek, K. Z. 2006, AJ, 131, 527

Jha, S., Riess, A. G., & Kirshner, R. P. 2007, ApJ

Knop, R. A., Aldering, G., Amanullah, R., Astier, P., Blanc, G., Burns, M. S., Conley, A., Deustua, S. E., Doi, M., Ellis, R., Fabbro, S., Folatelli, G., Fruchter, A. S., Garavini, G., Garmond, S., Garton, K., Gibbons, R., Goldhaber, G., Goobar, A., Groom, D. E., Hardin, D., Hook, I., Howell, D. A., Kim, A. G., Lee, B. C., Lidman, C., Mendez, J., Nobili, S., Nugent, P. E., Pain, R., Panagia, N., Pennypacker, C. R., Perlmutter, S., Quimby, R., Raux, J., Regnault, N., Ruiz-Lapuente, P., Sainton, G., Schaefer, B., Schahmaneche, K., Smith, E., Spadafora, A. L., Stanishev, V., Sullivan, M., Walton, N. A., Wang, L., Wood-Vasey, W. M., & Yasuda, N. 2003, ApJ, 598, 102

Krisciunas, K., Garnavich, P. M., Challis, P., Prieto, J. L., Riess, A. G., Barris, B., Aguilera, C., Becker, A. C., Blondin, S., Chornock, R., Clocchiatti, A., Covarrubias, R., Filippenko, A. V., Foley, R. J., Hicken, M., Jha, S., Kirshner, R. P., Leibundgut, B., Li, W., Matheson, T., Miceli, A., Miknaitis, G., Rest, A., Salvo, M. E., Schmidt, B. P., Smith, R. C., Sollerman, J., Spyromilio, J., Stubbs, C. W., Suntzeff, N. B., Tonry, J. L., & Wood-Vasey, W. M. 2005, AJ, 130, 2453

Landolt, A. U. 1983, AJ, 88, 439

—. 1992, AJ, 104, 340

Li, W., Filippenko, A. V., Chornock, R., Berger, E., Berlind, P., Calkins, M. L., Challis, P., Fassnacht, C., Jha, S., Kirshner, R. P., Matheson, T., Sargent, W. L. W., Simcoe, R. A., Smith, G. H., & Squires, G. 2003, PASP, 115, 453

Li, W., Filippenko, A. V., Gates, E., Chornock, R., Gal-Yam, A., Ofek, E. O., Leonard,

D. C., Modjaz, M., Rich, R. M., Riess, A. G., & Treffers, R. R. 2001a, PASP, 113, 1178

Li, W., Filippenko, A. V., & Riess, A. G. 2001b, ApJ, 546, 719

Livio, M. 2000, in Type Ia Supernovae, Theory and Cosmology. Edited by J. C. Niemeyer and J. W. Truran. Published by Cambridge University Press, 2000., p.33, 33–+

Matheson, T., Blondin, S., Foley, R. J., Chornock, R., Filippenko, A. V., Leibundgut, B., Smith, R. C., Sollerman, J., Spyromilio, J., Kirshner, R. P., Clocchiatti, A., Aguilera, C., Barris, B., Becker, A. C., Challis, P., Covarrubias, R., Garnavich, P., Hicken, M., Jha, S., Krisciunas, K., Li, W., Miceli, A., Miknaitis, G., Prieto, J. L., Rest, A., Riess, A. G., Salvo, M. E., Schmidt, B. P., Stubbs, C. W., Suntzeff, N. B., & Tonry, J. L. 2005, AJ, 129, 2352

Matheson, T., Filippenko, A. V., Barth, A. J., Ho, L. C., Leonard, D. C., Bershady, M. A., Davis, M., Finley, D. S., Fisher, D., González, R. A., Hawley, S. L., Koo, D. C., Li, W., Lonsdale, C. J., Schlegel, D., Smith, H. E., Spinrad, H., & Wirth, G. D. 2000a, AJ, 120, 1487

Matheson, T., Filippenko, A. V., Ho, L. C., Barth, A. J., & Leonard, D. C. 2000b, AJ, 120, 1499

Mulchaey, J. 2001, LDSS-2 User's Guide [LINK]

Nomoto, K., Umeda, H., Kobayashi, C., Hachisu, I., Kato, M., & Tsujimoto, T. 2000, in American Institute of Physics Conference Series, 35–52

Norgaard-Nielsen, H. U., Hansen, L., Jorgensen, H. E., Aragon Salamanca, A., & Ellis, R. S. 1989, Nature, 339, 523

Nugent, P., Kim, A., & Perlmutter, S. 2002, PASP, 114, 803

Oke, J. B., Cohen, J. G., Carr, M., Cromer, J., Dingizian, A., Harris, F. H., Labrecque, S., Lucinio, R., Schaal, W., Epps, H., & Miller, J. 1995, PASP, 107, 375

Padmanabhan, T. 2003, Phys. Rep., 380, 235

Peebles, P. J. & Ratra, B. 2003, Reviews of Modern Physics, 75, 559

Perlmutter, S., Aldering, G., Goldhaber, G., Knop, R. A., Nugent, P., Castro, P. G., Deustua, S., Fabbro, S., Goobar, A., Groom, D. E., Hook, I. M., Kim, A. G., Kim, M. Y., Lee, J. C., Nunes, N. J., Pain, R., Pennypacker, C. R., Quimby, R., Lidman, C., Ellis,

R. S., Irwin, M., McMahon, R. G., Ruiz-Lapuente, P., Walton, N., Schaefer, B., Boyle, B. J., Filippenko, A. V., Matheson, T., Fruchter, A. S., Panagia, N., Newberg, H. J. M., Couch, W. J., & The Supernova Cosmology Project. 1999, ApJ, 517, 565

Perlmutter, S., Pennypacker, C. R., Goldhaber, G., Goobar, A., Muller, R. A., Newberg, H. J. M., Desai, J., Kim, A. G., Kim, M. Y., Small, I. A., Boyle, B. J., Crawford, C. S., McMahon, R. G., Bunclark, P. S., Carter, D., Irwin, M. J., Terlevich, R. J., Ellis, R. S., Glazebrook, K., Couch, W. J., Mould, J. R., Small, T. A., & Abraham, R. G. 1995, ApJ, 440, L41

Phillips, M. M. 1993, ApJ, 413, L105

Prieto, J. L., Rest, A., & Suntzeff, N. B. 2006, ApJ, 647, 501

Renzini, A. 1996, in IAU Colloq. 145: Supernovae and Supernova Remnants, 77–+

Riess, A. G., Filippenko, A. V., Challis, P., Clocchiatti, A., Diercks, A., Garnavich, P. M., Gilliland, R. L., Hogan, C. J., Jha, S., Kirshner, R. P., Leibundgut, B., Phillips, M. M., Reiss, D., Schmidt, B. P., Schommer, R. A., Smith, R. C., Spyromilio, J., Stubbs, C., Suntzeff, N. B., & Tonry, J. 1998, AJ, 116, 1009

Riess, A. G., Filippenko, A. V., Li, W., Treffers, R. R., Schmidt, B. P., Qiu, Y., Hu, J., Armstrong, M., Faranda, C., Thouvenot, E., & Buil, C. 1999a, AJ, 118, 2675

Riess, A. G., Kirshner, R. P., Schmidt, B. P., Jha, S., Challis, P., Garnavich, P. M., Esin, A. A., Carpenter, C., Grashius, R., Schild, R. E., Berlind, P. L., Huchra, J. P., Prosser, C. F., Falco, E. E., Benson, P. J., Briceño, C., Brown, W. R., Caldwell, N., dell'Antonio, I. P., Filippenko, A. V., Goodman, A. A., Grogin, N. A., Groner, T., Hughes, J. P., Green, P. J., Jansen, R. A., Kleyna, J. T., Luu, J. X., Macri, L. M., McLeod, B. A., McLeod, K. K., McNamara, B. R., McLean, B., Milone, A. A. E., Mohr, J. J., Moraru, D., Peng, C., Peters, J., Prestwich, A. H., Stanek, K. Z., Szentgyorgyi, A., & Zhao, P. 1999b, AJ, 117, 707

Riess, A. G., Nugent, P. E., Gilliland, R. L., Schmidt, B. P., Tonry, J., Dickinson, M., Thompson, R. I., Budavári, T., Casertano, S., Evans, A. S., Filippenko, A. V., Livio, M., Sanders, D. B., Shapley, A. E., Spinrad, H., Steidel, C. C., Stern, D., Surace, J., & Veilleux, S. 2001, ApJ, 560, 49

Riess, A. G., Press, W. H., & Kirshner, R. P. 1996, ApJ, 473, 88

Riess, A. G., Strolger, L., Tonry, J., Casertano, S., Ferguson, H. C., Mobasher, B., Challis, P., Filippenko, A. V., Jha, S., Li, W., Chornock, R., Kirshner, R. P., Leibundgut, B.,

Dickinson, M., Livio, M., Giavalisco, M., Steidel, C. C., Benítez, T., & Tsvetanov, Z. 2004, ApJ, 607, 665

Riess, A. G., Strolger, L.-G., Casertano, S., Ferguson, H. C., Mobasher, B., Gold, B., Challis, P. J., Filippenko, A. V., Jha, S., Li, W., Tonry, J., Foley, R., Kirshner, R. P., Dickinson, M., MacDonald, E., Eisenstein, D., Livio, M., Younger, J., Xu, C., Dahlen, T., & Stern, D. 2006, ArXiv Astrophysics e-prints

Schechter, P. L., Mateo, M., & Saha, A. 1993, PASP, 105, 1342

Schmidt, B. P., Suntzeff, N. B., Phillips, M. M., Schommer, R. A., Clocchiatti, A., Kirshner, R. P., Garnavich, P., Challis, P., Leibundgut, B., Spyromilio, J., Riess, A. G., Filippenko, A. V., Hamuy, M., Smith, R. C., Hogan, C., Stubbs, C., Diercks, A., Reiss, D., Gilliland, R., Tonry, J., Maza, J., Dressler, A., Walsh, J., & Ciardullo, R. 1998, ApJ, 507, 46

Schmidt, G. D., Weymann, R. J., & Foltz, C. B. 1989, PASP, 101, 713

Sheinis, A. I., Bolte, M., Epps, H. W., Kibrick, R. I., Miller, J. S., Radovan, M. V., Bigelow, B. C., & Sutin, B. M. 2002, PASP, 114, 851

Spergel, D. N., Bean, R., Dore', O., Nolta, M. R., Bennett, C. L., Hinshaw, G., Jarosik, N., Komatsu, E., Page, L., Peiris, H. V., Verde, L., Barnes, C., Halpern, M., Hill, R. S., Kogut, A., Limon, M., Meyer, S. S., Odegard, N., Tucker, G. S., Weiland, J. L., Wollack, E., & Wright, E. L. 2006, ArXiv Astrophysics e-prints

Steinhardt, P. J. 2003, Royal Society of London Philosophical Transactions Series A, 361, 2497

Steinhardt, P. J. & Turok, N. 2002, Science, 296, 1436

—. 2005, New Astronomy Review, 49, 43

Stritzinger, M., Leibundgut, B., Walch, S., & Contardo, G. 2006, A&A, 450, 241

Stubbs, C. W. & Tonry, J. L. 2006, ApJ, 646, 1436

Sullivan, M., Le Borgne, D., Pritchet, C. J., Hodsman, A., Neill, J. D., Howell, D. A., Carlberg, R. G., Astier, P., Aubourg, E., Balam, D., Basa, S., Conley, A., Fabbro, S., Fouchez, D., Guy, J., Hook, I., Pain, R., Palanque-Delabrouille, N., Perrett, K., Regnault, N., Rich, J., Taillet, R., Baumont, S., Bronder, J., Ellis, R. S., Filiol, M., Lusset, V., Perlmutter, S., Ripoche, P., & Tao, C. 2006, ApJ, 648, 868

Tegmark, M., Strauss, M. A., Blanton, M. R., Abazajian, K., Dodelson, S., Sandvik, H., Wang, X., Weinberg, D. H., Zehavi, I., Bahcall, N. A., Hoyle, F., Schlegel, D., Scoccimarro, R., Vogeley, M. S., Berlind, A., Budavari, T., Connolly, A., Eisenstein, D. J., Finkbeiner, D., Frieman, J. A., Gunn, J. E., Hui, L., Jain, B., Johnston, D., Kent, S., Lin, H., Nakajima, R., Nichol, R. C., Ostriker, J. P., Pope, A., Scranton, R., Seljak, U., Sheth, R. K., Stebbins, A., Szalay, A. S., Szapudi, I., Xu, Y., Annis, J., Brinkmann, J., Burles, S., Castander, F. J., Csabai, I., Loveday, J., Doi, M., Fukugita, M., Gillespie, B., Hennessy, G., Hogg, D. W., Ivezić, Ž., Knapp, G. R., Lamb, D. Q., Lee, B. C., Lupton, R. H., McKay, T. A., Kunszt, P., Munn, J. A., O'Connell, L., Peoples, J., Pier, J. R., Richmond, M., Rockosi, C., Schneider, D. P., Stoughton, C., Tucker, D. L., vanden Berk, D. E., Yanny, B., & York, D. G. 2004, Phys. Rev. D, 69, 103501

Tonry, J. L., Schmidt, B. P., Barris, B., Candia, P., Challis, P., Clocchiatti, A., Coil, A. L., Filippenko, A. V., Garnavich, P., Hogan, C., Holland, S. T., Jha, S., Kirshner, R. P., Krisciunas, K., Leibundgut, B., Li, W., Matheson, T., Phillips, M. M., Riess, A. G., Schommer, R., Smith, R. C., Sollerman, J., Spyromilio, J., Stubbs, C. W., & Suntzeff, N. B. 2003, ApJ, 594, 1

Upadhye, A., Ishak, M., & Steinhardt, P. J. 2005, Phys. Rev. D, 72, 063501

Wade, R. A. & Horne, K. 1988, ApJ, 324, 411

Weinberg, S. 1989, Reviews of Modern Physics, 61, 1

Weller, J. & Albrecht, A. 2002, Phys. Rev. D, 65, 103512

Wood-Vasey, W. M., Miknaitis, G., Stubbs, C. W., Jha, S., Riess, A. G., Garnavich, P. M., Kirshner, R. P., Aguilera, C., Blackman, J. W., Becker, A. C., Blondin, S., Challis, P., Clocchiatti, A., Conley, A., Covarrubias, R., Davis, T. M., Filippenko, A. V., Foley, R. J., Garg, A., Hicken, M., Krisciunas, K., Leibundgut, B., Li, W., Matheson, T., Miceli, A., Narayan, G., Pignata, G., Prieto, J. L., Rest, A., Salvo, M. E., Schmidt, B. P., Smith, R. C., Sollerman, J., Spyromilio, J., Tonry, J. L., Suntzeff, N. B., & Zenteno, A. 2007, ApJ

Wood-Vasey, W. M., Wang, L., & Aldering, G. 2004, ApJ, 616, 339

York, D. G., Adelman, J., Anderson, Jr., J. E., Anderson, S. F., Annis, J., Bahcall, N. A., Bakken, J. A., Barkhouser, R., Bastian, S., Berman, E., Boroski, W. N., Bracker, S., Briegel, C., Briggs, J. W., Brinkmann, J., Brunner, R., Burles, S., Carey, L., Carr, M. A., Castander, F. J., Chen, B., Colestock, P. L., Connolly, A. J., Crocker,

J. H., Csabai, I., Czarapata, P. C., Davis, J. E., Doi, M., Dombeck, T., Eisenstein, D., Ellman, N., Elms, B. R., Evans, M. L., Fan, X., Federwitz, G. R., Fiscelli, L., Friedman, S., Frieman, J. A., Fukugita, M., Gillespie, B., Gunn, J. E., Gurbani, V. K., de Haas, E., Haldeman, M., Harris, F. H., Hayes, J., Heckman, T. M., Hennessy, G. S., Hindsley, R. B., Holm, S., Holmgren, D. J., Huang, C.-h., Hull, C., Husby, D., Ichikawa, S.-I., Ichikawa, T., Ivezić, Ž., Kent, S., Kim, R. S. J., Kinney, E., Klaene, M., Kleinman, A. N., Kleinman, S., Knapp, G. R., Korienek, J., Kron, R. G., Kunszt, P. Z., Lamb, D. Q., Lee, B., Leger, R. F., Limmongkol, S., Lindenmeyer, C., Long, D. C., Loomis, C., Loveday, J., Lucinio, R., Lupton, R. H., MacKinnon, B., Mannery, E. J., Mantsch, P. M., Margon, B., McGehee, P., McKay, T. A., Meiksin, A., Merelli, A., Monet, D. G., Munn, J. A., Narayanan, V. K., Nash, T., Neilsen, E., Neswold, R., Newberg, H. J., Nichol, R. C., Nicinski, T., Nonino, M., Okada, N., Okamura, S., Ostriker, J. P., Owen, R., Pauls, A. G., Peoples, J., Peterson, R. L., Petravick, D., Pier, J. R., Pope, A., Pordes, R., Prosapio, A., Rechenmacher, R., Quinn, T. R., Richards, G. T., Richmond, M. W., Rivetta, C. H., Rockosi, C. M., Ruthmansdorfer, K., Sandford, D., Schlegel, D. J., Schneider, D. P., Sekiguchi, M., Sergey, G., Shimasaku, K., Siegmund, W. A., Smee, S., Smith, J. A., Snedden, S., Stone, R., Stoughton, C., Strauss, M. A., Stubbs, C., SubbaRao, M., Szalay, A. S., Szapudi, I., Szokoly, G. P., Thakar, A. R., Tremonti, C., Tucker, D. L., Uomoto, A., Vanden Berk, D., Vogeley, M. S., Waddell, P., Wang, S.-i., Watanabe, M., Weinberg, D. H., Yanny, B., & Yasuda, N. 2000, AJ, 120, 1579

Zacharias, N., Urban, S. E., Zacharias, M. I., Wycoff, G. L., Hall, D. M., Monet, D. G., & Rafferty, T. J. 2004, AJ, 127, 3043
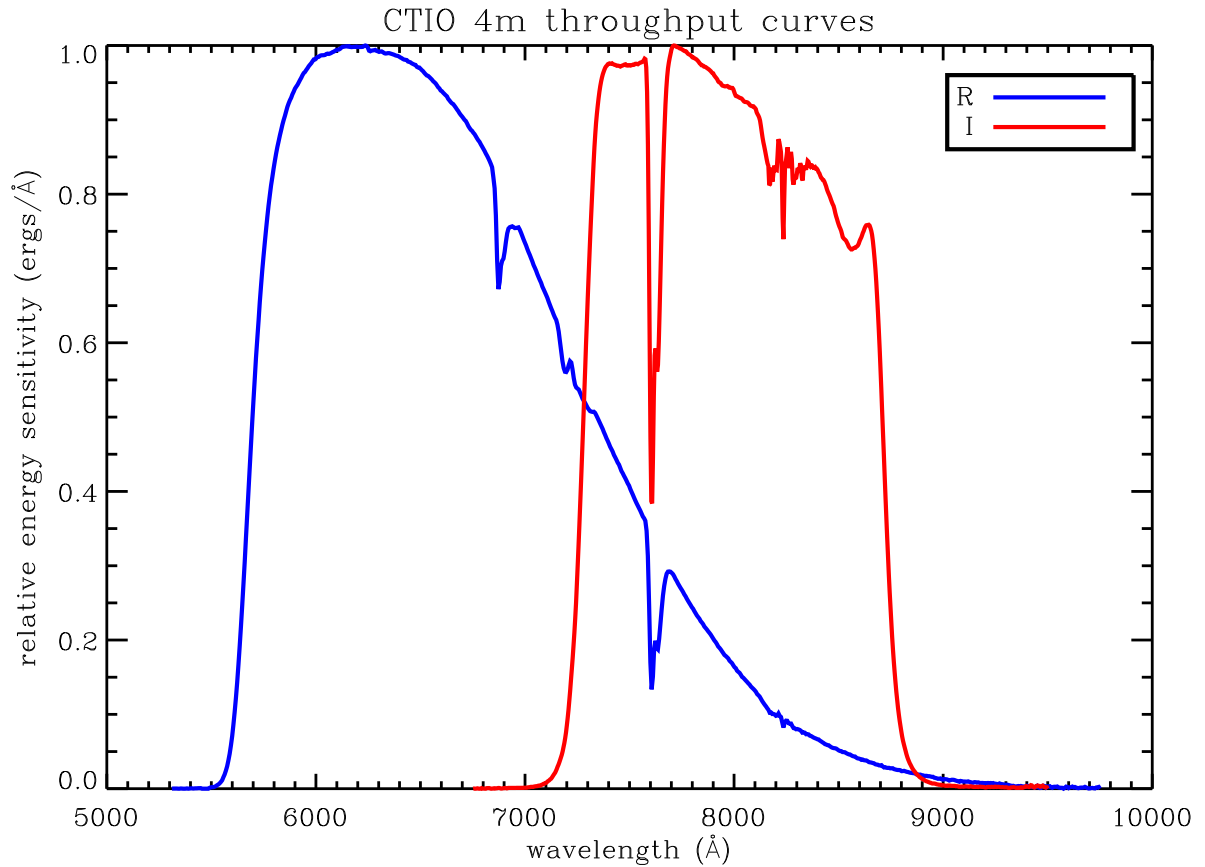
Fig. 13.— Throughput curves for the CTIO 4m R and I bandpasses. These represent the full system throughput, which includes the wavelength-dependence of: the CCD quantum efficiency, the optical filters, the aluminum reflectance for the mirrors in the 4m telescope and a model for the typical atmosphere transmissivity. The curves here are represented in relative energy sensitivity in ergs/Angstrom. Each curve has been normalized to unity at its peak.